Nonparametric maximum likelihood methods for binary response models with random coefficients

Jiaying Gu
Roger Koenker

NONPARAMETRIC MAXIMUM LIKELIHOOD METHODS FOR BINARY RESPONSE MODELS WITH RANDOM COEFFICIENTS

JIAYING GU AND ROGER KOENKER

ABSTRACT. Single index linear models for binary response with random coefficients have been extensively employed in many econometric settings under various parametric specifications of the distribution of the random coefficients. Nonparametric maximum likelihood estimation (NPMLE) as proposed by Cosslett (1983) and Ichimura and Thompson (1998), in contrast, has received less attention in applied work due primarily to computational difficulties. We propose a new approach to computation of NPMLEs for binary response models that significantly increase their computational tractability thereby facilitating greater flexibility in applications. Our approach, which relies on recent developments involving the geometry of hyperplane arrangements, is contrasted with the recently proposed deconvolution method of Gautier and Kitamura (2013). An application to modal choice for the journey to work in the Washington DC area illustrates the methods.

1. INTRODUCTION

Consider the linear index, random coefficient binary response model,

$$(1) \qquad y_i = 1\{x_i^\top \beta_i + w_i^\top \theta_0 \geqslant 0\}.$$

We observe covariates $x_i \in \mathbb{R}^{d+1}$, $w_i \in \mathbb{R}^p$, and the binary response, y_i. We will assume that the random parameters β_i are independent of both x_i and w_i and are drawn iidly from an unknown distribution F_0. The remaining Euclidean parameters, $\theta_0 \in \Theta \subset \mathbb{R}^p$ are fixed and also unknown. Our objective is to estimate the pair (θ_0, F_0) by maximum likelihood. This model encompasses many existing single index binary choice models in the literature. When the covariates x_i contain only an intercept term we have the simplest version of the semiparametric single index model considered in Cosslett (1983). When $d > 1$ and there are no other covariates w_i, it is the random coefficient single index model of Ichimura and Thompson (1998).

It is immediately apparent that the distribution of the β_i's is only identified up to a scale transformation of the coordinates of β, so without loss of generality we could impose the normalization that $\|\beta\| = 1$. An additional identification requirement noted by Ichimura and Thompson (1998) is that the distribution of β_i must have support on some hemisphere. This requirement will be fulfilled if the sign of one of the β coordinates is known, we will assume henceforth that the last entry of β is positive, so β_i's would be restricted to lie in the northern hemisphere. Under this additional assumption an alternative normalization simply takes the coordinate with the known sign to be 1 and focuses attention on the joint

DEPARTMENT OF ECONOMICS, UNIVERSITY OF TORONTO, TORONTO, ONTARIO, M5S 3G7, CANADA
DEPARTMENT OF ECONOMICS, UNIVERSITY COLLEGE LONDON, LONDON, WC1H OAX, UK

distribution of the remaining coordinates relative to it. In our modal choice application for example the price effect can be normalized to 1, and remaining covariate effects are interpreted relative to the effect of price. Henceforth, we shall assume that $x = (1, z_i^\top, -\nu_i)$ and $\beta_i = (\eta_i^\top, 1)$ with $\eta \in \mathbb{R}^d$, and estimation $F_0 = F_\beta$ is reduced to estimation of $F_0 = F_\eta$. Finally, it should be stressed from the outset that identification requires sufficient variability in x_i to trace out F_0 on its full support. These conditions will be made more explicit in the sequel.

We begin with a brief discussion of the simplest case in which there is only a univariate random coefficient as considered in the seminal paper of Cosslett (1983), a formulation that already illustrates many of the essential ideas. This is followed by a general treatment of the multivariate setting that draws on recent developments in combinatorial geometry involving "hyperplane arrangements." A discussion of identification and consistency is then followed by a brief description of some simulation experiments. Performance comparisons are made with the deconvolution approach of Gautier and Kitamura (2013). We conclude with an illustrative application to modal choice of commuters in the Washington DC area based on data from Horowitz (1993).

2. Univariate Randomness

In our simplest setting we have only a univariate random component and we observe thresholds, ν_i, and associated binary responses,

$$(2) \qquad\qquad y_i = 1(\eta_i \geqslant \nu_i) \quad i = 1, \cdots, n,$$

with η_i's drawn iidly from the distribution F_η and independently of the ν_i. In economic applications, with ν_i taken as a price the survival curve, $1 - F_\eta(\nu)$ can be interpreted as a demand curve, the proportion of the population willing to pay, ν. More generally, the single index model, might express $\nu_i = \nu(w_i, \theta)$ depending on other covariates, w_i and unknown parameters, θ. This is the context of Cosslett (1983) who focuses most of his attention on estimation of the distribution F_η employing the nonparametric maximum likelihood estimator (NPMLE) of Kiefer and Wolfowitz (1956). Estimation of the remaining parameters can be carried out by some form of profile likelihood, but we will defer such considerations. In biostatistics (2) is referred to as the current status model: we observe inspection times, ν_i, and a binary indicator, y_i, revealing whether an unobserved event time, η_i, has occurred prior to its associated inspection time, ν_i. Again, the objective is to estimate the distribution of the event times, F_η, by nonparametric maximum likelihood as described, for example, by Groeneboom, Jongbloed, and Witte (2010).

The geometry of maximum likelihood in this univariate setting is quite simple and helps to establish a heuristic for the general multivariate case. To illustrate the role of these intervals under the standard convention of the current status model, we can write,

$$\mathbb{P}(y = 1|\nu) = \int 1(\eta \leqslant \nu) dF_\eta(\eta).$$

Given a sample $\{(y_i, \nu_i)\ i = 1, \cdots, n\}$, this relation defines $n + 1$ intervals as illustrated for $n = 10$ in the upper panel of Figure 1. Each point defines a half line on $\mathbb{R}$; if $y_i = 1$ then the interval is $R_i = (-\infty, \nu_i]$, while if $y_i = 0$ the interval is $R_i = (\nu_i, \infty)$. Neglecting for the moment the possibility of ties, the R_i's form a partition of $n + 1$ intervals of $\mathbb{R}$, We will

denote these intervals by I_j, for $j = 1, \cdots, n+1$; they can be either closed, open or half open. We now define the associated counts,

$$c_j = \sum_{i=1}^{n} 1\{R_i \cap I_j \neq \emptyset\}$$

$$= \begin{cases} \sum_{i:y_i=0} 1\{v_i < v_{(j)}\} + \sum_{i:y_i=1} 1\{v_i \geqslant v_{(j)}\} & \text{for} \quad 1 \leqslant j \leqslant n \\ \sum_{i:y_i=0} 1\{v_i \leqslant v_{(n)}\} & \text{for} \quad j = n+1 \end{cases}$$

where $v_{(j)}$ is the j-th order statistic of the sample $\{v_1, \ldots, v_n\}$. Now suppose we assign probability mass, p_j to each of the intervals I_j, so that $p = \{p_1, \ldots, p_{n+1}\}$ in the n dimensional unit simplex, S_n. Then the contribution of the i-th data point to the likelihood is $\sum_j p_j 1\{R_i \cap I_j \neq \emptyset\}$. The nonparametric maximum likelihood estimator of F_η has the following essential features:

(1) Since the p_j's are assigned to intervals, it does not matter where mass is located within the intervals, as long as it is assigned to a point inside, in this sense the NPMLE, $\hat{F}_\eta$, is defined only on the sigma algebra of sets formed from the intervals,
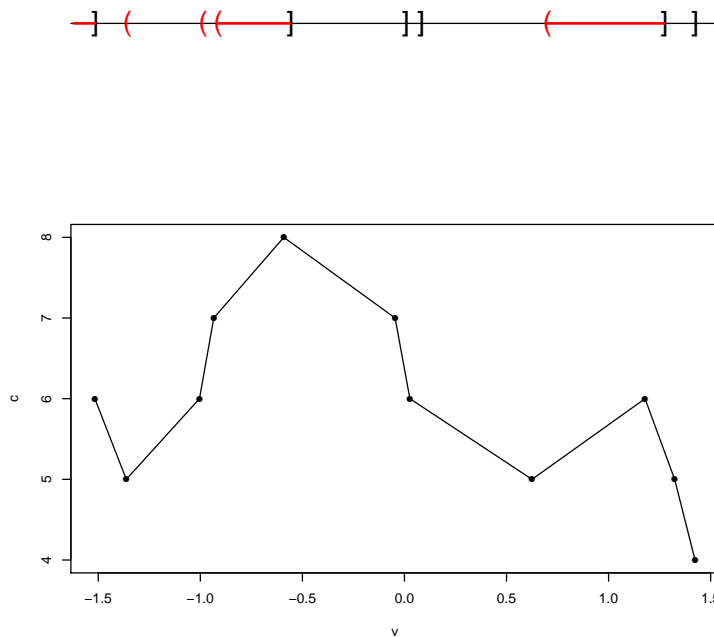

FIGURE 1. Intervals for a sample of 10 observations in the univariate Cosslett model. The intervals demarcated by the heavier (red) segments are local maxima, the number of counts for each interval is illustrated in the lower portion of the figure.

I_j. By convention we could assign the mass to the right end of each interval, but we should remember that this is only a convention. The MLE assigns mass to sets, not to points.

(2) Potential non-zero elements of p correspond to intervals I_j with corresponding c_j being a local maximum. Were this not the case, the likelihood could always be increased by transferring mass to adjacent intervals containing larger counts. Figure 1 plots values for the vector c. It is quite efficient to generate the vector c and find these local maxima even when n is very large.

These features suggest a convex optimization strategy for estimation of F_η. Since mass needs only to be assigned to the right endpoint of intervals that correspond to local maxima of the counts, we only need consider those potential support points. This serves as a dimension reduction device compared to considering all n original data points. However, in our experience, the number of potential support points of the distribution F_η identified in this manner still grows linearly with the sample size n, while the number of optimal support points identified by the maximum likelihood estimator grows more slowly. To determine which of our locally maximal intervals deserves positive mass and if so how much, we must solve,

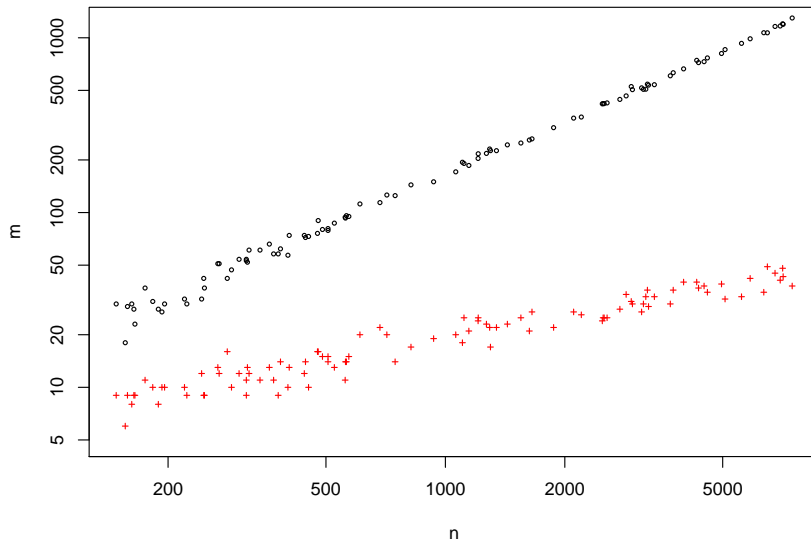$$\max_{f \in \mathcal{S}_{m-1}} \left\{ \sum_{i=1}^{n} \log g_i \mid Af = g \right\}$$

FIGURE 2. Number of local maxima of interval counts (black circles) and number of points of support of the optimal NPMLE solution (red pluses). The local maxima grow essentially linearly with sample size, while the number of support points in the NPMLE grow roughly logarithmically.

where $f = (f_j)$ denotes the mass assigned to the j-th order statistic of our reduced set of potential ν of cardinality m. The i-th coordinate of Af equals to $\sum_j 1\{\nu_{(j)} \leqslant \nu_i\}f_j$ if $y_i = 1$ and $\sum_j 1\{\nu_{(j)} > \nu_i\}f_j$ if $y_i = 0$. As first noted by Cosslett (1983), this problem turns out to be a special instance of the nonparametric maximum likelihood estimator described in Kiefer and Wolfowitz (1956). Noting that the problem is strictly concave in the g_i and subject only to linear equality and inequality constraints, it can be solved very efficiently, as noted by Koenker and Mizera (2014), by interior point methods as implemented for example in Mosek, the optimization framework developed by Andersen (2010). When this is carried out one finds that the number of support points of the estimated distribution, $\hat{F}_\eta$, is considerably smaller than the number of local maxima identified as candidates. Indeed, in contrast to the linear growth of the local maxima, the number of support points of the solutions to the NPMLE problem grows roughly like $\sqrt{n}$. This is illustrated in Figure 2, where we have generated standard Gaussian ν_i's and η_i's, for samples of size, $n = \exp(\xi)$ with $\xi \sim U[5, 9]$; round black points indicate the number of local maxima, while red plus points depict the number of optimal support points. This slow growth in the number of mass points selected by the NPMLE is consistent with prior experience with related methods for estimating smooth mixture models as described in Koenker and Mizera (2014) and Gu and Koenker (2016).

When we admit the possibility of ties in the ν_i's increased care is required to correctly count the number of observations allocated to each of the intervals. This is especially true when conflicting binary responses are observed at tied values of ν. In such cases it is convenient to shift locations, ν_i of the tied $y_i = 0$ observations slightly thereby restoring the uniqueness of the intervals.

3. Multivariate Randomness

The convenience of the univariate case is that there is a clear ordering of ν_i on $\mathbb{R}$, hence the partition is very easy to be characterized and enumerated. This seems to be lost once we encounter the multivariate case, however the bivariate current status and bivariate interval censoring models considered by Groeneboom and Jongbloed (2014) provide a valuable conceptual transition in which the intervals of the univariate setting are replaced by rectangles in the bivariate setting. Maathuis (2005) describes an effective algorithm for these models that shares some features with our approach.

To help visualize the geometry of the NPMLE in our more general setting with multivariate random coefficients we will first consider the bivariate case without any auxiliary covariates, w_i, and maintain the small sample focus of the previous section. Now, $x_i = (1, z_i, -\nu_i)^\top$ where z_i is a random scalar and $\eta_i \sim F_0$. The binary response is generated as,

$$\mathbb{P}(y_i = 1 | x_i) = \mathbb{P}(\eta_{1i} + z_i^\top \eta_{2i} - \nu_i \geqslant 0).$$

Each pair, (z_i, ν_i), defines a line that divides $\mathbb{R}^2$ into two halfspaces, an "upper" one corresponding to realizations of $y_i = 1$, and a "lower" one for $y_i = 0$. Let R_i denote these halfspaces and $F(R_i)$ be the probability assigned to each R_i by the distribution F. Our

objective is to estimate the distribution, F_0. The log likelihood of the observed sample is,

$$\ell(F) = \sum_{i=1}^{n} \log F(R_i).$$

As in the univariate case, the R_i partition the domain of β, however, now rather than intervals the partition consists of polygons formed by intersections of the R_i halfspaces. Adapting our counting method for intervals to these polygons, we seek to identify polygons whose counts are locally maximal. Within these maximal polygons the data is uninformative so again there is some inherent ambiguity about the nature of the NPMLE solutions. As in the one dimensional case this ambiguity can be resolved by adopting a selection rule for choosing a point within each polygon. As long as there is sufficient variability in the pairs (z_i, v_i)'s this ambiguity will vanish as the sample size grows as we will consider more formally in Section 4.

Figure 3 illustrates this partition with $n = 5$. The data for this example are given in Table 1.

	(Intercept)	z_i	v_i	y_i
$i = 1$	1.00	0.41	1.22	1
$i = 2$	1.00	0.40	0.36	0
$i = 3$	1.00	0.17	0.24	1
$i = 4$	1.00	-0.79	0.99	0
$i = 5$	1.00	-0.94	0.55	0

TABLE 1. Data for a toy example with $n = 5$

The half spaces $\{R_1, \ldots, R_n\}$ partition $\mathbb{R}^2$ into disjoint polygons $C_1, \ldots, C_M$. Since for each i, it has to be that $C_m \cap R_i = \emptyset$ or $C_m \cap R_i = C_m$, we can represent

$$F(R_i) = \sum_{j=1}^{M} p_j 1\{C_j \subset R_i\}$$

where p_j denotes the probability assigned to C_j, and we can express the log likelihood in terms of these probabilities, $p = (p_j)_{j=1:M}$,

$$\ell(p) = \sum_{i=1}^{n} \log \Big(\sum_{j=1}^{M} p_j 1\{C_j \subset R_i\} \Big).$$

The vector p must lie in the $M - 1$ dimensional unit simplex so we have a strictly concave objective function defined on a convex set that yields a unique solution. Just as in the univariate setting where we need not consider *all* intervals only those with locally maximal counts, we now need only consider polygons with locally maximal counts, thereby reducing the dimension, M, of the vector p.

We now illustrate how to find the maximal polygons for our toy example with $n = 5$. Figure 3 shows that there are three maximal polygons, all shaded and denoted as $\{C_1, C_2, C_3\}$. Polygon C_1 is the intersection of $\{R_1, R_3, R_4, R_5\}$, C_2 is the intersection of $\{R_1, R_2, R_4, R_5\}$ and C_3 is the intersection of $\{R_1, R_2, R_3\}$. Each is locally maximal in the
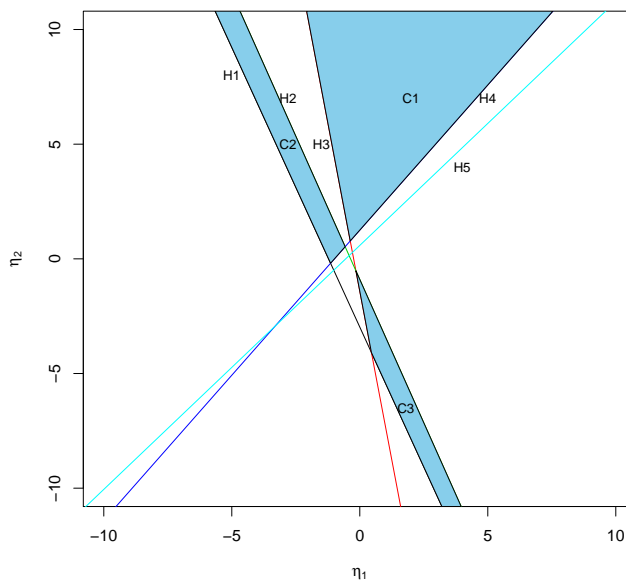
FIGURE 3. The polygons defined by a toy example with $n = 5$.

sense that they are formed by more intersecting halfspaces than any of their neighbours. The maximum likelihood estimator for p is defined as the maximizers of,

$$\max_{p \in \mathcal{S}_2} \log \left\{ (p_1 + p_2 + p_3)(p_2 + p_3)(p_1 + p_3)(p_1 + p_2)(p_1 + p_2) \right\}$$

which leads to the unique solution, $p_1 = p_2 = 1/2$ and $p_3 = 0$, and the optimal log-likelihood of $\log(1/4) = -1.3863$. We should again stress that although the mass associated with the two optimal polygons is uniquely determined by maximizing the likelihood, the position of the mass is ambiguous, confined only to the regions bounded by the two polygons.

As n grows the number of maximal polygons grows rapidly and finding all of them in the informal manner described above quickly becomes impractical. Fortunately, there is an extensive, relatively recent, combinatorial geometry literature on "hyperplane arrangements" that allows for efficient and tractable enumeration of the partition induced by any set of n hyperplanes in $\mathbb{R}^d$.

3.1. **Hyperplane Arrangement and Cell Enumeration.** Given a set of hyperplanes $H := \{H_1, H_2, \ldots, H_n\}$ in $\mathbb{R}^d$, it defines a partition of the space. In the computational geometry literature, this partition is called a hyperplane arrangement $\mathcal{A}(H)$. We first characterize the complexity of an arrangement by the following Lemma.

Lemma 1. *The number of cells of an arrangement of n hyperplanes in $\mathbb{R}^d$ is $\mathcal{O}(n^d)$.*

Proof. See Buck (1943), or for further elaboration Zaslavsky (1975). ∎

Remark. The worst case occurs when all n hyperplanes are in general position: a hyperplane arrangement $\mathcal{H} = \{H_1, \cdots, H_n\}$ in $\mathbb{R}^d$ is in general position if for $1 \leqslant k \leqslant< n$ any collection of k of them intersect in a $d - k$ dimensional hyperplane if $1 \leqslant k \leqslant d$ and if $k > d$ they have an empty intersection. In such cases the number of cells generated by the n hyperplanes is given by $\sum_{i=0}^{d} \binom{n}{i}$.

When $d = 2$ we have lines not hyperplanes. There are three basic elements in a line arrangement: vertices, edges and polygons. Vertices are the zero-dimensional points at which two or more lines intersect. Edges are the one-dimensional open line segments or open infinite rays that connect the vertex points. Faces, or cells, are the two-dimensional interiors of the bounded or unbounded convex polygons formed by the arrangement. If all lines $\{H_1, \ldots, H_n\}$ are in general positions, then the number of vertices is $\binom{n}{2}$, the number of edges is n^2 and the number of cells is $\binom{n}{2} + n + 1 = \mathcal{O}(n^2)$. When lines are not in general position, which is likely to occur in many empirical settings, the complexity of the line arrangement is characterized in Alexanderson and Wetzel (1981). We return to this possibility in Section 3.4 below. $\blacksquare$

Our first objective is to enumerate all the polytopes, or cells, formed by a given arrangement, denoted as $\{C_1, C_2, \ldots, C_M\}$. For each cell C_j we can define a sign vector $s_j \in \{\pm 1\}^n$ whose i-th element is,

$$s_{ij} := \begin{cases} 1 & \text{for } Z_i^\top \eta - v_i > 0 \\ -1 & \text{for } Z_i^\top \eta - v_i < 0, \end{cases}$$

where $Z_i := \{1, z_i^\top\}^\top$ and η is an arbitrary interior point of C_j. In this form the sign vector ignores the information in y_i, but this can easily be rectified by flipping the sign of the i-th element in the sign vector. We will define the modified sign vector to be $\tilde{s}_j$ with

$$\tilde{s}_{ij} := \begin{cases} 1 & \text{for } y_i = 1, Z_i^\top \eta - v_i > 0 \\ -1 & \text{for } y_i = 1, Z_i^\top \eta - v_i < 0 \\ 1 & \text{for } y_i = 0, Z_i^\top \eta - v_i < 0 \\ -1 & \text{for } y_i = 0, Z_i^\top \eta - v_i > 0 \end{cases}$$

Each cell is uniquely identified by its sign vector and an associated interior point η. The interior point η is arbitrary, but since the likelihood is determined only by the probability mass assigned to each cell, we need only find a valid interior point η_j for each polytope C_j. This can be accomplished by examining solutions to the linear program,

$$(3) \qquad \{\eta_j^*, \epsilon_j^*\} = \underset{\eta, \epsilon}{\operatorname{argmax}} \left\{ S_j(Z\eta - v) \geqslant \epsilon \mathbf{1}_n, 0 \leqslant \epsilon \leqslant 1 \right\}.$$

Here, S_j is a $n \times n$ diagonal matrix with diagonal elements $\{s_{1j}, s_{2j}, \ldots, s_{nj}\}$. It can be seen that η_j is a valid interior point of C_j if and only if $\epsilon_j^* > 0$. The upper bound for ϵ can be changed to any arbitrary positive number, thereby influencing which interior point found as the optimal solution.

The linear program (3) thus provides a means to check if a particular configuration of the sign vector is compatible with a given hyperplane arrangement. A brute force way to enumerate all cells in the arrangement is to exhaust all possible sign vectors in the set $\{\pm 1\}^n$, of which there are 2^n elements. For each element we could solve the linear programming problem and check the existence of a valid interior point. This is obviously

computationally ridiculous and unnecessary since the maximum number of cells generated by a n-hyperplane arrangement in $\mathbb{R}^d$ is only of order n^d as stated in Lemma 1. Avis and Fukuda (1996) were apparently the first to develop an algorithm for cell enumeration that runs in time proportional to the maximum number of polygons of an arrangement. Sleumer (1998) improved upon their reverse search algorithm. More recently, Rada and Černý (2018) have proposesd an incremental enumeration algorithm that is asymptotically equivalent to the Avis-Fukuda's reverse search algorithm, but is demonstrably faster in finite samples. The most costly component of the Rada-Černý algorithm involves solving the linear programs (3). We will briefly describe the Rada-Černý Incremental Enumeration (IE) algorithm and then discuss a modified version that we have developed that reduces the complexity of IE algorithm by an order of magnitude n.

As the name suggests the IE algorithm adds hyperplanes one at a time to enumerate all sign vectors of an arrangement in n iterations. Let s^k denote a sign vector of length k in the set of possible vectors $\{\pm 1\}^k$. In the k-th step of the algorithm with $1 < k \leqslant n$, we have as input the sign vectors s^{k-1} for all existing cells formed by the first $k-1$ hyperplanes and their associated interior points collected in the set η^{k-1}; we will index its elements by ℓ. At each iteration we do the following:

Algorithm 1: Iteration of the Incremental Enumeration algorithm

---

   input : The existing sets of sign vectors s^{k-1} and interior points η^{k-1} and the new
             hyperplane H_k.
   output: The new sets of sign vectors s^k and the interior points η^k.

     (a) For each elements in the set s^{k-1}, say s_ℓ^{k-1}, define the new sign vector
         $s_\ell^k := \{s_\ell^{k-1}, 2 \times 1\{Z_k^\top \eta_\ell^{k-1} - \nu_k > 0\} - 1\}\}$.
     (b) For each element s_ℓ^k obtained from (a), solve the linear program defined in (3)
         with the sign vector $\check{s}_\ell^k := \{s_\ell^{k-1}, 1 - 2 \times 1\{Z_k^\top \eta_\ell^{k-1} - \nu_k > 0\}\}$, store the optimal
         solutions $\check{\eta}_\ell^k$ and $\check{\epsilon}_\ell^k$.
     (c) Define the set $s^k := \{s_\ell^k, \forall l\} \cup \{\check{s}_\ell^k, \forall \ell \text{ such that } \check{\epsilon}_\ell^k > 0\}$ and the set
         $\eta^k := \{\eta_\ell^k, \forall \ell\} \cup \{\check{\eta}_\ell^k, \forall \ell \text{ such that } \check{\epsilon}_\ell^k > 0\}$.

The algorithm can be initiated with an arbitrary point η_1^1, as long as it does not fall exactly on any of the hyperplane. When the first hyperplane H_1 is added, it necessarily partitions the space $\mathbb{R}^d$ into two parts. Since η_1^1 has to belong to one of the parts, we define $s_1^1 = 2 \times 1\{Z_1^\top \eta_1^1 - \nu_1 > 0\} - 1$. For the other half, one solves the linear program (3) with $S = s_2^1 = -s_1^1$ and records the solution as η_2^1; defining $s^1 := \{s_1^1, s_2^1\}$ and $\eta^1 := \{\eta_1^1, \eta_2^1\}$ which become the input for the first iteration of the IE algorithm. The order of addition of the hyperplanes does not influence the final output.

Figure 3.1 illustrates the idea of the iterative algorithm for a linear arrangement. The input at the third iteration is illustration in the left panel. There are four polygons that partition $\mathbb{R}^2$ determined by the arrangement $\{H_1, H_2\}$. The interior points are labeled by their associated sign vector represented by the symbols $\pm$. When H_3 is added, step one of the algorithm determines s_ℓ^3 for $\ell = 1, \ldots, 4$. Step two looks for the new polygons created by adding H_3, which crosses through polygons A,C,D, dividing each into two parts, and

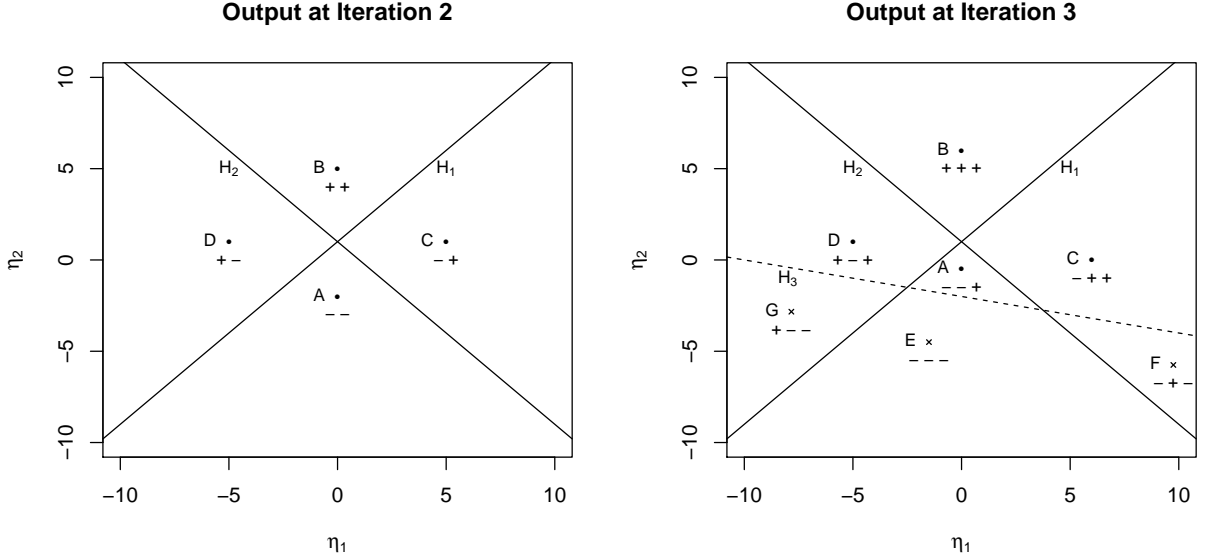**Output at Iteration 2**   **Output at Iteration 3**

FIGURE 4. Illustration of the IE algorithm: the left panel plots the output of the second iteration. The two hyperplane involves are $H_1 = \{(\eta_1, \eta_2) \mid -\eta_1 + \eta_2 - 1 = 0\}$ and $H_2 = \{(\eta_1, \eta_2) \mid \eta_1 + \eta_2 - 1 = 0\}$. The right panel plots the output of the third iteration, the additional hyperplane $H_3 = \{(\eta_1, \eta_2) \mid 0.2\eta_1 + \eta_2 + 2 = 0\}$.

leads to the three new polygons E,F and G. Polygon B lies strictly on one side of H_3, hence it is not divided.

The most time-consuming step is (b) in each iteration, although each LP problem can be very quickly solved as long as the dimension d is moderate. We have to solve $\sum_{i=0}^{d} \binom{k-1}{i} = \mathcal{O}((k-1)^d)$ such problems in the worst case as a consequence of Lemma 1. Together, for all n iterations, this requires $\mathcal{O}(n^{d+1})$ for any arrangement in $\mathbb{R}^d$.

3.2. **Dimension reduction based on locally maximal polygons.** Once we have enumerated all the cells, an adjacency matrix A can be created with dimension $n \times M$ and elements taking values in $\{0, 1\}$. The j-th column of the A matrix is the corresponding modified sign vector $\tilde{s}_j$ of cell C_j, except that we replace all -1 values by 0. As we have already noted the number of columns of the A matrix, M is of order n^d which increases rapidly as n increases, so it is important to try to reduce the number of candidate cells as much as possible. To achieve a dimension reduction we need to eliminate cells that are not locally maximal, that is cells that have neighbours with larger cell counts. Define the M-vector c whose elements denote the column sums of the adjacency matrix A. corresponding to each cell $\{C_1, \ldots, C_M\}$. The cells C_j and C_k are neighbours if their sign vector differ by exactly one sign. For each cell C_j we can define its set of neighbours N_j. The cardinality of any set

N_j is at most n. The following result determines the set of columns in the matrix A that will be locally maximal and therefore constitute candidate supporting cells of the NPMLE.

Theorem 1. *Any cell C_j with associated count, c_j, that is strictly smaller than any of the counts of the cells in its neighbouring set N_j is assigned zero probability mass by the NPMLE.*

Proof. Suppose the NPMLE assigned positive probability mass p to such an C_j. By re-assigning the probability mass p to the cell in the set N_j with a larger count the likelihood could be strictly increased, hence p must be zero. ∎

Remark. It is perhaps worth noting at this point that the cell, or cells, possessing the globally maximal cell count constitute an exhaustive solution to the maximum score problem posed in Manski (1975), that is, any element of the set $\{C_k : k \in \mathcal{K}\}$ for $\mathcal{K} = \{k : c_k = \max\{c_j : j = 1, \cdots, M\}\}$ is an argmax of the maximum score objective function. Likewise, any other locally maximal cell is a region in which the maximal score estimator may become marooned in the search for a global maximum. ∎

3.3. **Acceleration of the Rada-Černý algorithm.** The main motivation of our modification of the IE algorithm is to reduce the number of LP problems that need to be solved. To this end we apply a "zone theorem" for hyperplane arrangements of Edelsbrunner, Seidel, and Sharir (1993) to show that the number of necessary LP problems in step (b) of the IE algorithm can be reduced from $\mathcal{O}(n^{d+1})$ to $\mathcal{O}(n^d)$.

Theorem 2. *For any set of H of n hyperplanes in $\mathbb{R}^d$ and any hyperplane $H' \notin H$, denote the total number of cells in the arrangement of $\mathcal{A}(H)$ that intersects with H' as h, then*

$$h \leqslant \sum_{i=0}^{d-1} \binom{n}{i}$$

with the equality achieved when all hyperplanes in the set $H \cup \{H'\}$ are in general position.

Proof. *Theorem 2.1 in Edelsbrunner, Seidel, and Sharir (1993) with $k = 0$, yields,*

$$h \leqslant \binom{d-1}{0}\binom{n}{d-1} + \sum_{0 \leqslant j < d-1} \binom{j}{0}\binom{n}{j} = \sum_{i=0}^{d-1} \binom{n}{i}.$$

∎

Theorem 2 implies that when we add a new distinct hyperplane to an existing arrangement with $k-1$ hyperplanes, it crosses at most $\mathcal{O}((k-1)^{d-1})$ cells. For line arrangements this implies that a newly added distinct line crosses at most k polygons. Only these k polygons will generate a new cell, hence in step (b) of the k-th iteration of the IE algorithm, we need only to solve at most k LPs provided we can efficiently find the relevant k sign vectors for these crossed cells. We first give details for line arrangement in Algorithm 2 and then discuss how to extend this approach to general case in $\mathbb{R}^d$.

Algorithm 2 describes how to achieve this when all lines are in general position. In each iteration, Step (b.1) finds the subset of sign vectors in s^{k-1} whose corresponding cell intersects with the new line H_k. Step (b.2) then finds the interior points for all the newly created cells by solving the associated LPs. When lines are not in general position (i.e.

Algorithm 2: Accelerated Incremental Enumeration algorithm ($d = 2$)

---

   input : The existing set of sign vectors s^{k-1} and interior points η^{k-1} and the new line H_k.

  output: The new set of sign vectors s^k and interior points η^k.

   (a) For each element in the set s^{k-1}, say s_ℓ^{k-1}, define the new sign vector
$s_\ell^k := \{s_\ell^{k-1}, 2 \times 1\{Z_k^\top \eta_\ell^{k-1} - \nu_k > 0\} - 1\}\}$.

 (b.1) Find the set of vertices $\{t_1, t_2, \ldots, t_{k-1}\}$, where t_j is the vertex of the intersection of H_k and H_j for $1 \leqslant j < k$. Let $u_j^{k-1} := \{sgn\{Z_i^\top t_j - \nu_i\}\}_{i=1,2,\ldots,k-1}$. By the definition of a vertex, the j-th entry of u_j^{k-1} is zero and the remainder take values in $\{+1, -1\}$. Define u_{j+}^{k-1} to be identical to u_j^{k-1} except that its j-th entry is replaced by $+1$ and u_{j-}^{k-1} to be identical to u_j^{k-1} except that its j-th entry is replaced by -1. Let $u^{k-1} := \{u_{j-}^{k-1}, u_{j+}^{k-1}\}_{j=1,2,\ldots,k-1}$ and $\mathcal{Z}^{k-1} := u^{k-1} \cap s^{k-1}$ and denote the corresponding set of interior points as $\check{\eta}^{k-1}$.

 (b.2) For each element in the set $\mathcal{Z}^{k-1}$, say $\mathcal{Z}\ell^{k-1}$, solve the linear program defined in (3) with the sign vector $\tilde{s}_\ell^k := \{\mathcal{Z}\ell^{k-1}, 1 - 2 \times 1\{Z_k^\top \check{\eta}_\ell^{k-1} - \nu_k > 0\}\}$, store the optimal solutions $\tilde{\eta}_\ell^k$.

  (c) Define the set $s^k := \{s_\ell^k, \forall l\} \cup \{\tilde{s}_\ell^k, \forall \ell\}$ and the set $\eta^k := \{\eta_\ell^k, \forall \ell\} \cup \{\tilde{\eta}_\ell^k, \forall \ell\}$.

---

more than two lines cross at the same vertex) more entries in the vector u_j^{k-1} will be zero, and the set $\mathcal{Z}^{k-1}$ can be constructed in a similar fashion, as noted in the next subsection.

   The AIE algorithm is easily adapted to the general case with hyperplanes in $\mathbb{R}^d$, at least when the arrangement is in general position. When a new hyperplane H_k is added, the set of vertices is determined by the intersection of H_k and any $d-1$ hyperplanes in the set $\{H_1, H_2, \ldots, H_{k-1}\}$. When hyperplanes are in general positions, there will be $\binom{k-1}{d-1}$ of these for $k \geqslant d$. Each of these vertices provide sign constraints on the cells that hyperplane H_k crosses, which allows us to determine a subset of s^{k-1} to be passed into step (b.2). For $1 < k < d$ the set of vertices is empty and we proceed to step (b.2) to process all elements in s^{k-1}.

3.4. **Treatment of various forms of degeneracy.** If the arrangement H is not in general position, Algorithm 2 must be adapted to cope with this. Alexanderson and Wetzel (1981) consider cell enumeration for $d = 2$ and $d = 3$, our implementation of the algorithm provisionally treats only the $d = 2$ case of line arrangements. In higher dimensions, degeneracy becomes quite delicate and constitutes a subject for future research. Random perturbation of the covariate data is an obvious alternative strategy for circumventing such degeneracy. Even for line arrangements there are several cases to consider:

  (1) If $H_k \in \{H_1, \ldots, H_{k-1}\}$ for any k, then (b.1) and (b.2) can be skipped since if the new line coincides with one of the existing ones since no new cells are created.

  (2) If H_k is parallel to any existing lines $\{H_1, \ldots, H_{k-1}\}$ the cardinality of the set of vertices will be smaller than $k-1$, but no modification of the algorithm is required.

(3) If H_k crosses a vertex that already exists, then more than one entry in u_j^{k-1} will be zero. Suppose there are a such zeros, then the zero entries must be replaced with elements in $\{\pm 1\}^a$ to construct the set u^{k-1}.

4. Identification and Strong Consistency

We now introduce formal conditions needed for identification of the parameters of interest (θ_0, F_0) for model (1) and to establish consistency of the nonparametric maximum likelihood estimator $(\hat\theta_n, \hat F_n)$. In this section, we will revert to the notation of our original model 1 with the normalization that $\|\beta\| = 1$.

Assumption 1. *The random vectors (x_i, w_i) and β_i are independent and the matrix $[X \vdots W]$ has full column rank.*

Assumption 2. *The parameter space Θ is a compact subset of a Euclidean space and $\theta_0 \in \Theta$. Let the set $\mathcal{F}$ be space of probability distribution for β_i supported on a d-dimensional unit sphere. Furthermore, there exists a vector $c \neq 0$ such that $\mathbb{P}_F(c^\top \beta_i > 0) = 1$ for all $F \in \mathcal{F}$.*

Assumption 3. *The distribution of (z_i, v_i) is absolutely continuous on $\mathbb{R}^d$ and $w^\top \theta$ is absolutely continuous; both possess an everywhere positive density.*

Versions of the foregoing assumptions are commonly invoked in the semiparametric single index binary choice model literature. Some relaxation of Assumption 1 is possible while still securing point identification of (θ_0, F_0). The normalization in Assumption 2 is commonly imposed in all binary choice models including the parametric models. This turns out to be convenient since the space $\mathcal{F}$ is then compact. The restriction that the distribution of β_i allocates all its probability mass to some hemisphere is specific for the random coefficient model to secure point identification. This is also imposed in Ichimura and Thompson (1998). Assumption 3 requires sufficient variability of the covariates to trace out F_0 on its full support. Note that it does not require all elements in w_i to have an absolutely continuous distribution with full support hence it allows for discrete covariates to be included in the model.

Theorem 3. *Under Assumptions 1-3, (θ_0, F_0) is identified.*

Proof. Define $p(y = 1|x, w, \theta, F) = \mathbb{P}_F(\{\beta : x^\top \beta \geqslant -w^\top \theta\})$ for any $(\theta, F) \in \Theta \times \mathcal{F}$. We first show that if θ_0 is known, then $p(y = 1|x, w, \theta_0, F) = p(y = 1|x, w, \theta_0, F_0)$ almost surely implies $F = F_0$. The argument follows the proof of Theorem 1 in Ichimura and Thompson (1998), mainly elaborating it to incorporate the profile likelihood estimation of the fixed parameter, θ_0.

Under Assumption 1, the equality $p(y = 1|x, w, \theta_0, F) = p(y = 1|x, w, \theta_0, F_0)$ implies that for all (x, t) where $t := -w^\top \theta_0$,

$$\mathbb{P}_F(\{\beta : x^\top \beta \geqslant t\}) = \mathbb{P}_{F_0}(\{\beta : x^\top \beta \geqslant t\})$$

as long as the support of t contains zero which holds under Assumption 3, we can apply the Cramér-Wold device and conclude that $F = F_0$.

Now suppose there exists $\theta \neq \theta_0$ such that for some $F \in \mathcal{F}$

$$(4) \qquad p(y = 1 | x, w, \theta, F) = p(y = 1 | x, w, \theta_0, F_0) \qquad \text{almost surely.}$$

Consider initially $d = 1$, and denote $x = (1, z)$ so the support of β is the unit circle in $\mathbb{R}^2$. Notice that the orientation of the line $\{\beta : \beta_1 + z\beta_2 = -w^\top\theta\}$ is solely determined by z and its intersection with the horizontal axis is solely determined by $-w^\top\theta$. Fix z and choose $w = w_1$ such that $w_1^\top\theta > 0$, $w_1^\top(\theta - \theta_0) > 0$ and the hyperplane $\{\beta : \beta_1 + z\beta_2 = -w_1^\top\theta\}$ is tangent to the unit circle as illustrated by the solid red line in Figure 5. Such a w_1 always exists under Assumption 3 that $w^\top\theta$ has full support. Then equality (4) implies that

$$1 = \mathbb{P}_F(\{\beta : \beta_1 + z\beta_2 \geqslant -w_1^\top\theta\}) = \mathbb{P}_{F_0}(\{\beta : \beta_1 + z\beta_2 \geqslant -w_1^\top\theta_0\})$$

Since $w_1^\top(\theta - \theta_0) > 0$, the line $\{\beta : \beta_1 + z\beta_2 = -w_1^\top\theta_0\}$ indicated by the dashed red line in Figure 5 intersects with the unit circle at two points, say a and b. The above equality also implies that the distribution F_0 puts zero probability mass on the shortest arc that connects a and b on the unit circle. Now since z has full support under Assumption 3, we can change z such that the two parallel hyperplanes rotate together to cover all directions. Applying the above argument for all such z leads to the conclusion that the distribution F_0 puts zero probability on the entire support of β, leading to a contradiction. Extending the argument to $d > 1$ is straightforward since under Assumption 3 z has full support. Together with the full column rank condition on $[X \dot{:} W]$ under Assumption 1, we conclude that z covers all possible directions in $\mathbb{R}^d$. ∎

Remark. If elements of x_i are endogenous but there exists a vector of instruments r_i and a complete model relating x_i and r_i is specified, for instance $x_i = \Psi r_i + e_i$, then we can rewrite model (1) as

$$y_i = 1\{\beta_{1i} + e_i^\top\beta_{-1,i} + r_i^\top\Psi^\top\beta_{-1,i} + w_i^\top\theta \geqslant 0\}$$

Thus, we can redefine the random intercept as $\beta_{1i} + e_i^\top\beta_{-1,i}$ and the remaining random coefficients accordingly, denoting by $\beta_{-1,i}$ the vector of β excluding the first component, and we are back to the original model (1). There is also a recent literature emphasizing on set identification of (θ_0, F_0) where an explicit model between x_i and r_i is not imposed. See Chesher and Rosen (2014) for a detailed discussion. ∎

Having established identification of the model structure (θ_0, F_0), we now turn our attention to the asymptotic behavior of the maximum likelihood estimator of (θ_0, F_0),

$$(\hat{\theta}_n, \hat{F}_n) = \underset{\Theta \times \mathcal{F}}{\operatorname{argmax}} \frac{1}{n} \sum_{i=1}^{n} y_i \log[\mathbb{P}_F(H(x_i, w_i, \theta))] + (1 - y_i)\log[1 - \mathbb{P}_F(H(x_i, w_i, \theta))]$$

where we denote the set $\{\beta : x_i^\top\beta + w_i^\top\theta \geqslant 0\}$ by $H(x_i, w_i, \theta)$. For any fixed n and θ, the collection of half spaces $H(x_i, w_i, \theta)$ defines a partition on the support of β, denoted as $\{C_1, \ldots, C_M\}$. Define a matrix A of dimension $n \times M$, whose entries takes the form $a_{ij} = 1\{C_j \subset H(x_i, w_i, \theta)\}$ for $y_i = 1$ and $a_{ij} = 1 - 1\{C_j \subset H(x_i, w_i, \theta)\}$ for $y_i = 0$. Let p be a vector in the unit simplex such that p_j corresponds to the probability assigned to the polytope C_j, the maximum likelihood estimator for F for a fixed θ, denoted as F_θ, is the
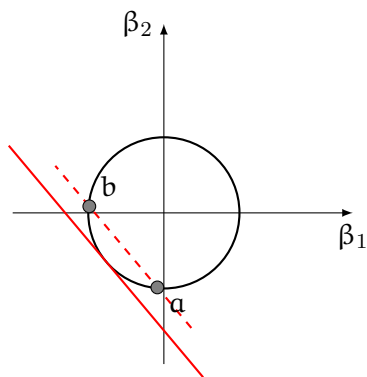
FIGURE 5. Joint identification of (θ_0, F_0).

solution to the following constrained optimization problem,

$$\min \left\{ -\frac{1}{n} \sum_{i=1}^{n} \log g_i \mid g_i = \sum_j a_{ij} p_j, \sum_j p_j = 1, p_j \geqslant 0 \right\}$$

The dual problem, which is usually more efficiently solved since M is typically much larger than n, can be shown to be

$$\max \left\{ \sum_{i=1}^{n} \log \nu_i \mid \sum_{i=1}^{n} a_{ij} \nu_i \leqslant n \text{ for all } j \right\}$$

In this formulation the problem appears to resemble the dual form of the NPMLE for general mixture models as considered by Lindsay (1983) and Koenker and Mizera (2014). Despite this resemblance, there are several fundamental differences that lead to special features of the binary response NPMLE. First, in classical mixture models the number of constraints in the dual problem is typically infinite dimensional. As a consequence it is conventional to impose a finite grid for the potential mass points of the mixing distribution to obtain a computationally practical approximation. The number of grid points should typically grow together with sample size n to achieve a good approximation. In contrast, in the binary response setting once n is fixed, the matrix A is determined by the arrangement and the solution of p is exact for any n. There is no need to impose a grid on the support of the parameters which is very convenient especially when the dimension of β is large. Second, the arrangement also provides a unique geometric underpinning which leads to an equivalence class of solutions for the maximum likelihood estimator. Once the convex program determines the optimal allocation $\hat{p}$, the data offers no information on how the probability masses $\hat{p}_j$, should be distributed on the polytope C_j. In this sense the NPMLE $\hat{F}_n$ yields a set-valued solution; in the application section we illustrate the implications of this fact for prediction of marginal effects. The maximum likelihood estimator for θ is found by maximizing the profile likelihood.

We now establish the consistency of the maximum likelihood estimator. The argument follows Kiefer and Wolfowitz (1956) and Chen (2017). Our argument relaxes some of the assumptions employed in prior work, in particular Assumption 4, in Ichimura and Thompson

(1998). Let $\mathcal{F}_0$ be the set of all absolutely continuous distribution on the support of β; $\mathcal{F}_0$ is a dense subset of $\mathcal{F}$.

Lemma 2. *Under assumption 1-3, for any given $\gamma = (\theta, F) \in \Theta \times \mathcal{F}_0$, let $\gamma_n = (\theta_n, F_n)$ be any sequence in $\Theta \times \mathcal{F}$ such that $\gamma_n \to \gamma$, then*

$$\lim_{\gamma_n \to \gamma} \mathbb{P}_{F_n}(H(x, w, \theta_n)) = \mathbb{P}_F(H(x, w, \theta)) \quad a.s.$$

Proof. For all $F \in \mathcal{F}_0$, since $w^\top \theta$ is continuous in θ, then there exists an $N_1 > 0$ such that for $n \geqslant N_1$, $|\mathbb{P}_F(H(x, w, \theta_n)) - \mathbb{P}_F(H(x, w, \theta))| < \epsilon$. By the Portmanteau Theorem, for any $F \in \mathcal{F}_0$, we also have that $F_n \to F$ implies $\mathbb{P}_{F_n}(H(x, w, \theta)) \to \mathbb{P}_F(H(x, w, \theta))$. That means there exists $N_2 > 0$ such that for $n \geqslant N_2$, $|\mathbb{P}_{F_n}(H(x, w, \theta)) - \mathbb{P}_F(H(x, w, \theta))| < \epsilon$. Therefore, $|\mathbb{P}_{F_n}(H(x, w, \theta_n)) - \mathbb{P}_F(H(x, w, \theta))| < 2\epsilon$ for n large enough. Since ϵ is arbitrary, it follows that $\lim_{\gamma_n \to \gamma} \mathbb{P}_{F_n}(H(x, w, \theta_n)) = \mathbb{P}_F(H(x, w, \theta))$ almost surely. ∎

Define the function $p(y, x, w, \gamma) := y\mathbb{P}_F(H(x, w, \theta)) + (1-y)(1 - \mathbb{P}_F(H(x, w, \theta)))$, and for any subset $\Gamma \subset \Theta \times \mathcal{F}$, let $p(y, x, w, \Gamma) = \sup_{\gamma \in \Gamma} p(y, x, w, \gamma)$. Let ρ be a distance on $\Theta \times \mathcal{F}$. This ρ can be the Euclidean distance on Θ together with any metric on F that metrises weak convergence of F. For any $\epsilon > 0$ let $\Gamma_\epsilon(\gamma^*) = \{\gamma : \rho(\gamma, \gamma^*) < \epsilon\}$ be an open ball of radius ϵ centered at γ^*.

Lemma 3. *Under Assumption 1-3, for any $\gamma \neq \gamma^*$, there exists an $\epsilon > 0$ such that*

$$\mathbb{E}^*\{[\log\{p(y, x, w, \Gamma_\epsilon(\gamma))/p(y, x, w, \gamma^*)\}]^+\} < \infty$$

where $\mathbb{E}^*$ denotes expectations taken with respect to $p(y, x, w, \gamma^*)$.

Proof. Since $0 \leqslant \mathbb{P}_F(H(x, w, \theta)) \leqslant 1$ for all $(\theta, F) \in \Theta \times \mathcal{F}$, we have

$$p(1, x, w, \Gamma_\epsilon(\gamma))/p(1, x, w, \gamma^*) \leqslant 1/\mathbb{P}_{F_0}(H(x, w, \theta_0)$$

and

$$p(0, x, w, \Gamma_\epsilon(\gamma))/p(0, x, w, \gamma^*) \leqslant 1/(1 - \mathbb{P}_{F_0}(H(x, w, \theta_0))$$

and consequently,

$$\mathbb{E}^*\{[\log\{p(y, x, w, \Gamma_\epsilon(\gamma))/p(y, x, w, \gamma^*)\}]^+\} \leqslant \int \Big\{ -\mathbb{P}_{F_0}(H(z, w, \theta_0)) \log \mathbb{P}_{F_0}(H(z, w, \theta_0)$$

$$- (1 - \mathbb{P}_{F_0}(H(z, w, \theta_0))) \log(1 - \mathbb{P}_{F_0}(H(z, w, \theta_0))) \Big\} dG(z) < \infty$$

where G denotes the joint distribution of (x, w). ∎

Theorem 4. *If $\{(y_i, x_i, w_i) : i = 1, 2, \cdots, n\}$ is an i.i.d sample from $p(y, x, w, \theta_0, F_0)$, under Assumptions 1-3, then $(\hat{\theta}_n, \hat{F}_n)$ is strongly consistent.*

Proof. Let $\gamma \neq \gamma^*$. Note that $\log\{p(y, x, w, \Gamma_\epsilon(\gamma))/p(y, x, w, \gamma^*)\}$ is a monotone increasing function of ϵ. Lemma 2 implies that $\lim_{\epsilon \downarrow 0} p(y, x, w, \Gamma_\epsilon(\gamma)) = p(y, x, w, \gamma)$, and dominated convergence implies that

$$\lim_{\epsilon \downarrow 0} E^*\{[\log\{p(y, x, w, \Gamma_\epsilon(\gamma))/p(y, x, w, \gamma^*)\}]^+\} = E^*\{[\log\{p(y, x, w, \gamma)/p(y, x, w, \gamma^*)\}]^+\}.$$

Lemma 2 and Fatou's Lemma then imply that

$$\liminf_{\epsilon \downarrow 0} E^*\{[\log\{p(y,x,w,\Gamma_\epsilon(\gamma))/p(y,x,w,\gamma^*)\}]^-\} \geqslant E^*\{[\log\{p(y,x,w,\gamma)/p(y,x,w,\gamma^*)\}]^-\}.$$

Monotonicity of $\log\{p(y,x,w,\Gamma_\epsilon(\gamma))/p(y,x,w,\gamma^*)\}$ in ϵ ensures that the limit exists, so,

$$\lim_{\epsilon \downarrow 0} E^*[\log\{p(y,x,w,\Gamma_\epsilon(\gamma))/p(y,x,w,\gamma^*)\}] \leqslant E^*[\log\{p(y,x,w,\gamma)/p(y,x,w,\gamma^*)\}] < 0.$$

Strict inequality holds by Jensen's inequality and the identification result in Theorem 3. Thus, for any $\gamma \neq \gamma^*$, there exists $\epsilon_\gamma > 0$ such that

$$E^*[\log\{p(y,x,w,\Gamma_{\epsilon_\gamma}(\gamma))/p(y,x,w,\gamma^*)\}] < 0$$

Now for any $\epsilon > 0$, the complementary set $(\Gamma_\epsilon(\gamma^*))^c$ is compact and is covered by $\cup_{\gamma \in (\Gamma_\epsilon(\gamma^*))^c} \Gamma_{\epsilon_\gamma}(\gamma)$, hence there exists a finite subcover, $\Gamma_1, \Gamma_2, \ldots, \Gamma_J$ such that for each j,

$$E^*[\log\{p(y,x,w,\Gamma_j)/p(y,x,w,\gamma^*)\}] < 0.$$

By the strong law of large numbers, as $n \to \infty$,

$$\sup_{\gamma \in (\Gamma_\epsilon(\gamma^*))^c} \frac{1}{n} \sum_i \log\{p(y_i,x_i,w_i,\gamma)/p(y_i,x_i,w_i,\gamma^*)\}$$

$$\leqslant \max_{j=1,\ldots,J} \frac{1}{n} \sum_i \log\{p(y_i,x_i,w_i,\Gamma_j)/p(y_i,x_i,w_i,\gamma^*)\}$$

$$\overset{a.s}{\to} \max_{j=1,\ldots,J} E^*[\log\{p(y,x,w,\Gamma_j)/p(y,x,w,\gamma^*)\}] < 0.$$

Since ϵ is arbitrarily chosen, this implies that $(\hat{\theta}_n, \hat{F}_n) \to (\theta_0, F_0)$ almost surely when $n \to \infty$. Note that we allow $E^*[\log\{p(y,x,w,\Gamma_j)/p(y,x,w,\gamma^*)\}]$ to be minus infinity when invoking the strong law based on the following argument. For any j,

$$\frac{1}{n} \sum_i \log\{p(y_i,x_i,w_i,\Gamma_j)/p(y_i,x_i,w_i,\gamma^*)\}$$

$$= \frac{1}{n} \sum_i \left[\log\{p(y_i,x_i,w_i,\Gamma_j)/p(y_i,x_i,w_i,\gamma^*)\}\right]^+ - \frac{1}{n} \sum_i \left[\log\{p(y_i,x_i,w_i,\Gamma_j)/p(y_i,x_i,w_i,\gamma^*)\}\right]^-.$$

Lemma 3 implies that

$$\frac{1}{n} \sum_i \left[\log\{p(y_i,x_i,w_i,\Gamma_j)/p(y_i,x_i,w_i,\gamma^*)\}\right]^+ \overset{a.s.}{\to} E^*\{[\log\{p(y_i,x_i,w_i,\Gamma_j)/p(y_i,x_i,w_i,\gamma^*)\}]^+\}.$$

It remains to show that

$$\frac{1}{n} \sum_i \left[\log\{p(y_i,x_i,w_i,\Gamma_j)/p(y_i,x_i,w_i,\gamma^*)\}\right]^- \overset{a.s.}{\to} E^*\{[\log\{p(y,x,w,\Gamma_j)/p(y,x,w,\gamma^*)\}]^-\}.$$

Suppose the right hand side is finite, then we can invoke the strong law. Alternatively, suppose $E^*\{[\log\{p(y,x,w,\Gamma_j)/p(y,x,w,\gamma^*)\}]^-\} = \infty$. Denote the random variable

$$\mathcal{R} := [\log\{p(y,x,w,\Gamma_j)/p(y,x,w,\gamma^*)\}]^-,$$

we have $\mathcal{R} \geqslant 0$ and $\mathsf{E}\mathcal{R} = \infty$. Let M be a constant, we have $\mathsf{E}[\min\{\mathcal{R}, \mathsf{M}\}] < \infty$ if $\mathsf{M} < \infty$ and $\mathsf{E}[\min\{\mathcal{Z}, \mathsf{M}\}] \to \infty$ as $\mathsf{M} \to \infty$. Then for every M,

$$\frac{1}{n}\sum_i \mathcal{Z}_i \geqslant \frac{1}{n}\sum_i \min\{\mathcal{Z}_i, \mathsf{M}\} \overset{a.s.}{\to} \mathsf{E}[\min\{\mathcal{Z}, \mathsf{M}\}].$$

Assembling the foregoing, we have,

$$\frac{1}{n}\sum_i \left[\log\{p(y_i, x_i, w_i, \Gamma_j)/p(y_i, x_i, w_i, \gamma^*)\} \right]^- \overset{a.s.}{\to} \mathsf{E}^*\{[\log\{p(y, x, w, \Gamma_j)/p(y, x, w, \gamma^*)\}]^-\}$$

as required.   ∎

5. Some Simulation Evidence

In this section we report on some very limited simulation experiments designed to compare performance of our NPMLE method with the recent proposal by Gautier and Kitamura (2013). The Gautier and Kitamura estimator may be viewed as a deconvolution procedure defined on a hemisphere in $\mathbb{R}^d$, and has the notable virtue that it can be computed in closed form via elegant Fourier-Laplace inversion formulae. A downside of the approach is that it involves several tuning/truncation parameters that seem difficult to select. In contrast the optimization required by our NPMLE is tuning parameter free, and the likelihood interpretation of the resulting convex optimization problem offers the opportunity to formulate extended versions of the problem containing additional fixed parameters that may be estimated by conventional profile likelihood methods.

To facilitate the comparison with Gautier and Kitamura (2013) we begin by considering the simulation setting of their paper. Rows of the design matrix, X are generated as $(1, x_{1i}, x_{2i})$ with standard Gaussian x_{ij}, and then normalized to have unit length. The random coefficients, β are generated from the two point distribution that puts equal mass on the points, $(0.7, -0.7, 1)$ and $(-0.7, 0.7, 1)$. The sample size is 500. Estimation imposes the condition that the third coordinate of β is 1, and interest focuses on estimating the distribution of the first two coordinates. After some experimentation with the author's Matlab code we have implemented a version of the Gautier and Kitamura (2013) estimator in R. We initially set the truncation and trimming parameters for the estimator as suggested in Gautier and Kitamura (2013), and we plot contours of the resulting density estimator in Figure 6. The discrete mass points of the data generating process are depicted as red circles in this figure. It may be noted that the estimated GK contours tend to concentrate the mass too much toward the origin. In an attempt to correct this bias effect, we experimented with increasing the truncation parameters to increase the flexibility of the sieve expansion. Figure 8 illustrates the contours of the fit with $T = 3$ replaced by $T = 7$. The two most prominent modes are now much closer to the discrete mass points of the process generating the data, but there is some cost in terms of increased variability. In Figure 7 we illustrate estimated mass points as well as contours of the NPMLE of the random coefficient density after convolution with a bivariate Gaussian distribution with diagonal covariance matrix with entries $(0.04, 0.04)$. The NPMLE is extremely accurate in this, somewhat artificial discrete setting. '

A somewhat more challenging setting for the NPMLE, also taken from Gautier and Kitamura (2013), involves random coefficients that are generated from a mixture of two
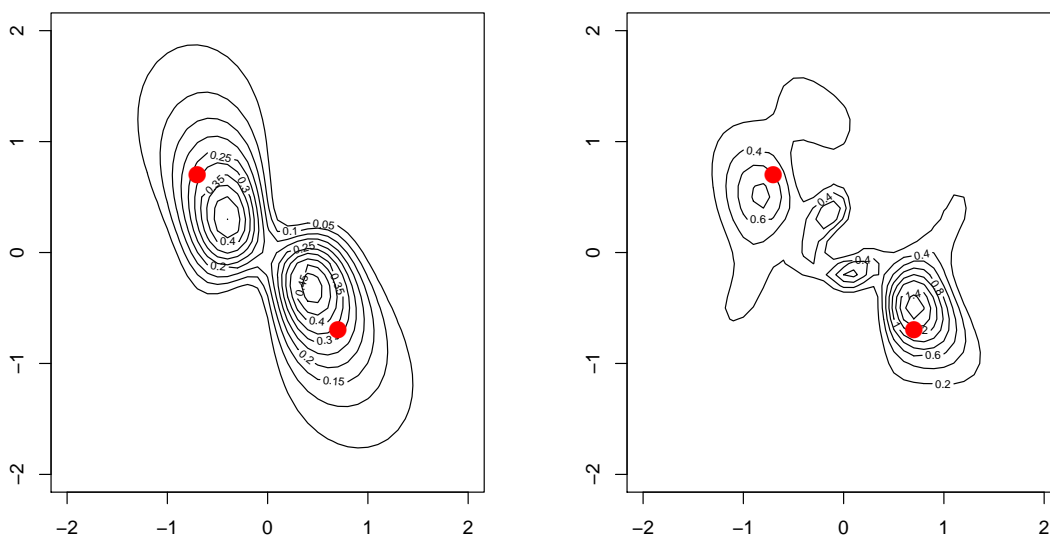
FIGURE 6. Contour plots of Gautier and Kitamura estimated density for the discrete simulation setting with η generated with equal probability from the two points $(0.7, -0.7)$ and $(-0.7, 0.7)$ indicated by the red circles. In the left panel the sieve dimension is set at the default value $\mathsf{T} = 3$, while in the right panel it is increase to $\mathsf{T} = 7$.

bivariate Gaussians with the same centers as in the previous case, but now both with variances 0.3, and covariance 0.15 for each of the equally weighted components. In Figure 8 we depict the density contours of the Gautier-Kitamura estimator with the contours of the true density of the random coefficients shown in grey. Again, it is apparent that the truncated basis expansion tends to shrink the mass of the estimated distribution toward the origin. In Figure 9 we illustrate estimated mass points as well as contours of the smoothed NPMLE density after convolution with a bivariate Gaussian distribution with diagonal covariance matrix with entries $(0.04, 0.04)$. The contours of the true density of the random coefficients are again depicted by the grey contours with centers indicated by the two red circles. The unsmoothed NPMLE has discrete mass points indicated by the blue circular regions in the figure. The smoothing introduces a tuning parameter into the NPMLE fit, but it should be stressed that prior to the convolution step to impose the smoothing there is no tuning parameter selection required. Clearly, there is more dispersion as we might expect in the NPMLE discrete solution, but the smoothed estimate quite accurately captures the two modes of the random coefficient density.

One swallow doesn't make a summer, so we have carried out two small simulation experiments to compare performance of the various estimators under consideration under both of the foregoing simulation settings. In the first experiment data is generated in accordance
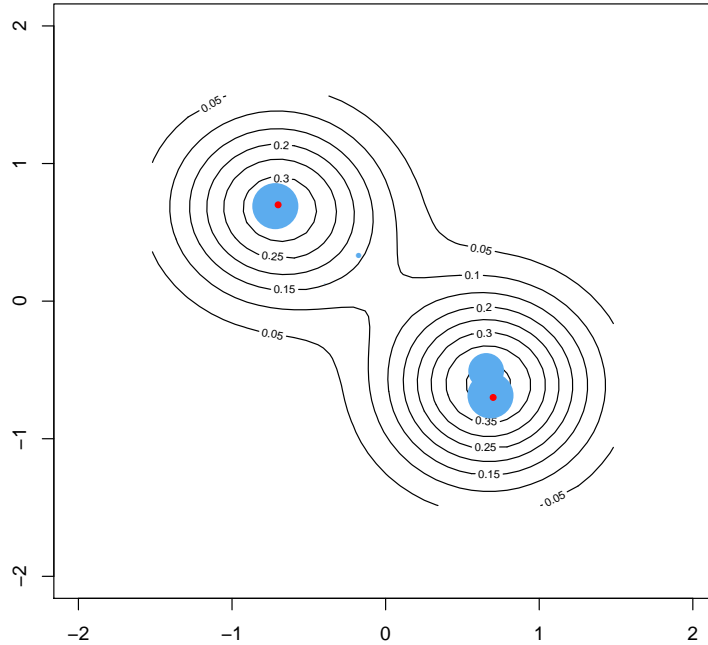
FIGURE 7. Msss points and smoothed contours of the NPMLE for the discrete Gautier-Kitamura simulation setting with mass concentrated at $(0.7, -0.7)$ and $(-0.7, 0.7)$ as indicated by the red circles. The mass points of the NPMLE are indicated by the solid blue circles, and contours of a smoothed version of the NPMLE based a Gaussian kernel with bandwidth 0.2.

with the two point discrete distribution taken from Gautier and Kitamura with sample size $n = 500$. Four estimators are considered: two variants of the NPMLE, one smoothed the other not, the Gautier-Kitamura estimator with default tuning parameter selection, and the classical logistic regression estimator. For each estimator we compute predicted probabilities for a fresh sample of 500 x observations also drawn from the same Gaussian distribution generating the data used for estimation. Table 2 reports mean absolute and root mean squared errors for the predicted probabilities for the 100 replications of the experiment. The discrete NPMLE is the clear winner, with its smoothed version performing only slightly better than the Gautier-Kitamura deconvolution procedure, the logit estimator is the clear loser.

Skeptical minds may, correctly, regard the two point distribution simulation setting as "too favorable" to the NPMLE since it is known to deliver a relatively sparse discrete estimate. Thus, it is of interest to see how our comparison would look when the true random coefficient distribution is itself smooth.
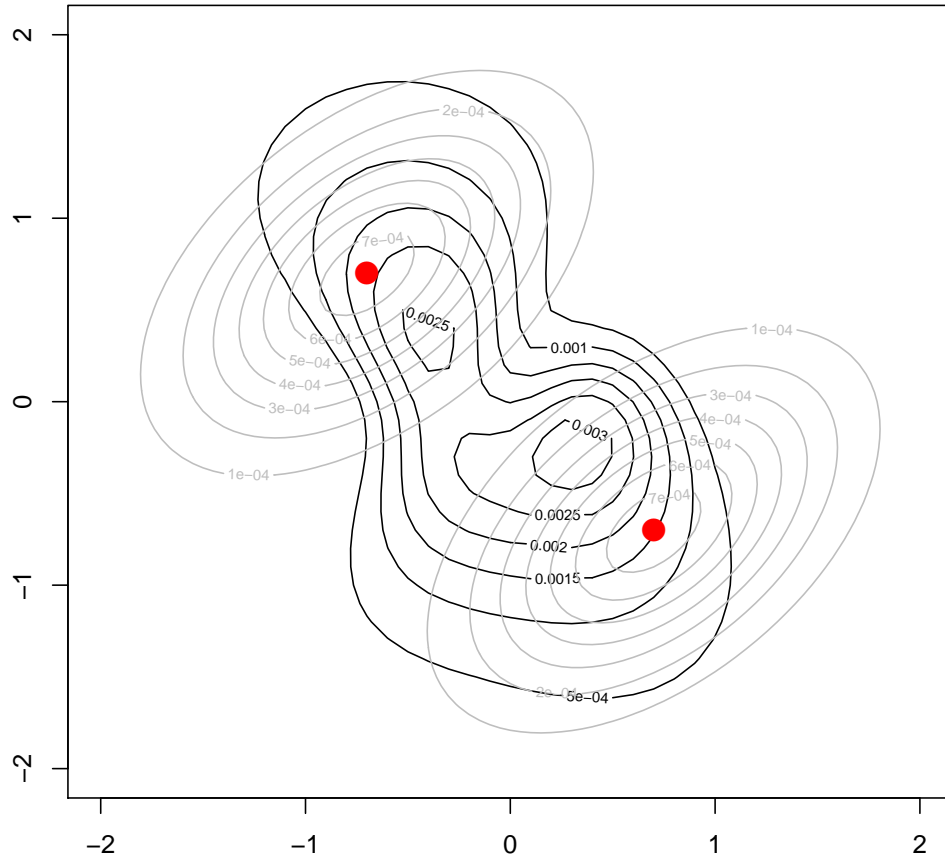
FIGURE 8. Gautier-Kitamura contours for a sample from the smooth bimodal bivariate distribution: The true distribution of the random coefficients is a Gaussian location mixture with two components each with variance 0.3, covariance 0.15 and means $(0.7, -0.7)$ and $(-0.7, 0.7)$. Contours of the true density are indicated in grey with respective means by the solid red circles.

	GK	NPMLE	NPMLEs	Logit
MAE	0.1333	0.0868	0.1274	0.1753
RMSE	0.1705	0.1576	0.1726	0.2150

TABLE 2. Bivariate Point Mass Simulation Setting: Mean Absolute and Root Mean Squared Errors of Predicted Probabilities
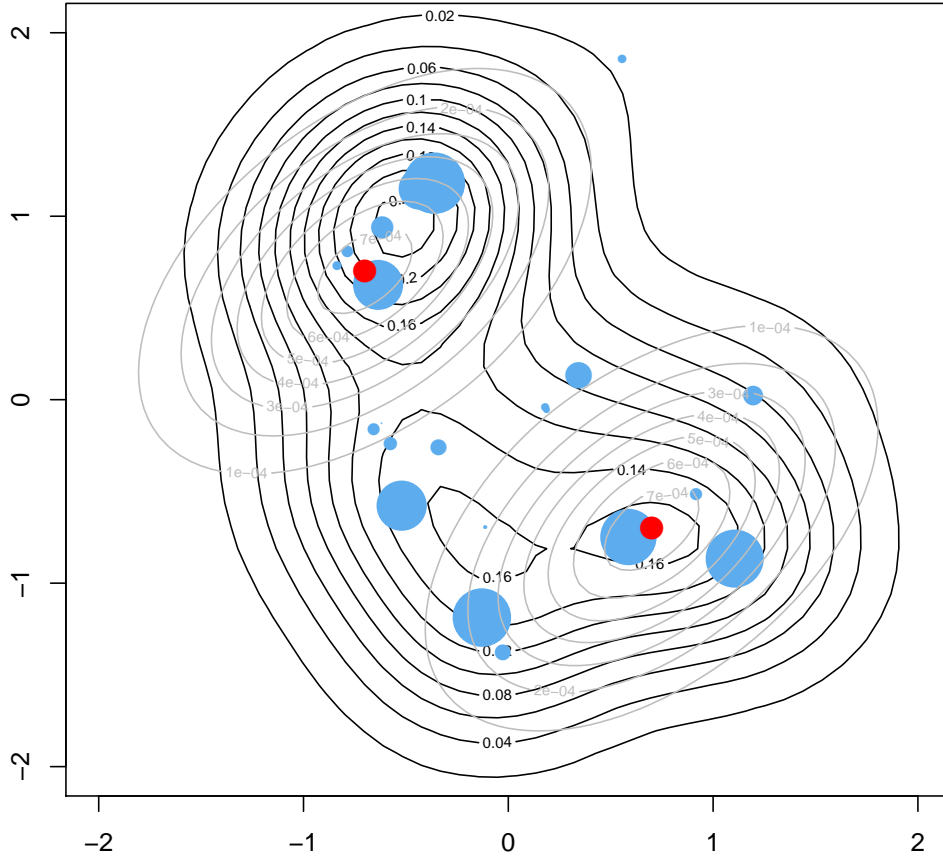
FIGURE 9. The NPMLE for a sample from a smooth bivariate distribution: The true distribution of the random coefficients is a Gaussian location mixture with two components each with variance 0.3, covariance 0.15 and means $(0.7, -0.7)$ and $(-0.7, 0.7)$. Contours of the true density are indicated in grey with respective means by the solid red circles. The mass points of the unsmoothed NPMLE are indicated by the solid blue circles whose areas depict associated mass. Contours of the smoothed NPMLE are shown in black.

Table 3 reports mean absolute and root mean squared errors for the predicted probabilities for the 100 replications of the new setting with the location mixture of Gaussians. Again, the NPMLE is the clear winner, but now its smoothed version performs somewhat better than the unsmoothed version although both do better than the Gautier-Kitamura deconvolution procedure.

	GK	NPMLE	NPMLEs	Logit
MAE	0.1288	0.0592	0.0475	0.0709
RMSE	0.1440	0.0748	0.0594	0.0896

TABLE 3. Bivariate Gaussian Simulation Setting: Mean Absolute and Root Mean Squared Errors of Predicted Probabilities

6. AN APPLICATION TO MODAL CHOICE

In this section we revisit the modal choice model of Horowitz (1993). The data consists of 842 randomly sampled observations of individuals' transportation choices for their daily journey to work in the Washington DC metro area. Following Horowitz, we focus on the binary choice of commuting to work by automobile versus public transit. In addition to the individual mode choice variable, y_i, taking the value 1 if an automobile is used for the journey to work and 0 if public transit is taken, we observe the number of cars owned by the traveller's household ($AUTOS$), the difference in out-of-vehicle ($DOVTT$) and in in-vehicle travel time ($DIVTT$). Differences are expressed as public transit time minus automobile time in minutes per trip. The corresponding differences in transportation cost, $DCOST$, public transit fare minus automobile travel cost is measured in cents per trip. We have omitted the variable $DIVTT$ from our analysis since it had no significant impact on modal choice in prior work, see Table 2 of Horowitz (1993) for estimation results using various parametric and semiparametric models. Although our methodology can accommodate additional x_i variables with random coefficients it becomes considerably more difficult to visualize distributions of random coefficients F_η in higher dimensions. Other control variables in the vector w_i could also be accommodated, but the application doesn't offer obvious candidates.

We consider the following random coefficient binary choice model:

$$\mathbb{P}(y_i = 1 \mid x_i, v_i, AUTOS_i = k) = \int 1\{x_i^\top \eta_i - v_i \geqslant 0\} dF_{\eta,k}$$

where $x_i = (1, DOVTT_i)$ and $v_i = DCOST_i/100$ and $\eta_i = \{\eta_{1i}, \eta_{2i}\}$. We have normalized the coefficient of v_i to be 1, since v_i represents a negative price, transit fare minus automobile cost. Under this normalization, the coefficient η_{2i} has a direct interpretation as the commuter's value of travel time in dollars/hour. The coefficient η_1 obviously has the same units as v_i, and can be interpreted as a threshold – setting a critical value for v_i above which the subject decides to commute by automobile, and below which he chooses to take public transit, assuming that the time differential is negligble. Auto ownership is a discrete variable, taking values between 0 and 7. Households with 3 cars or more commute exclusively by automobile, so we only consider subjects with fewer than 3 cars, a subsample containing about 90% of the data. Since car ownership is plausibly an endogenous decision and may act as a proxy for wealth of the household and potential constraint on the travellers' mode choices, we estimate distinct distributions of the random coefficients for subjects with zero, one and two cars. Figure 10 provides scatter plots of $DOVTT$ and $DCOST$ for $k \in \{0, 1, 2\}$, distinguishing auto and transit commuters by open and filled circles.
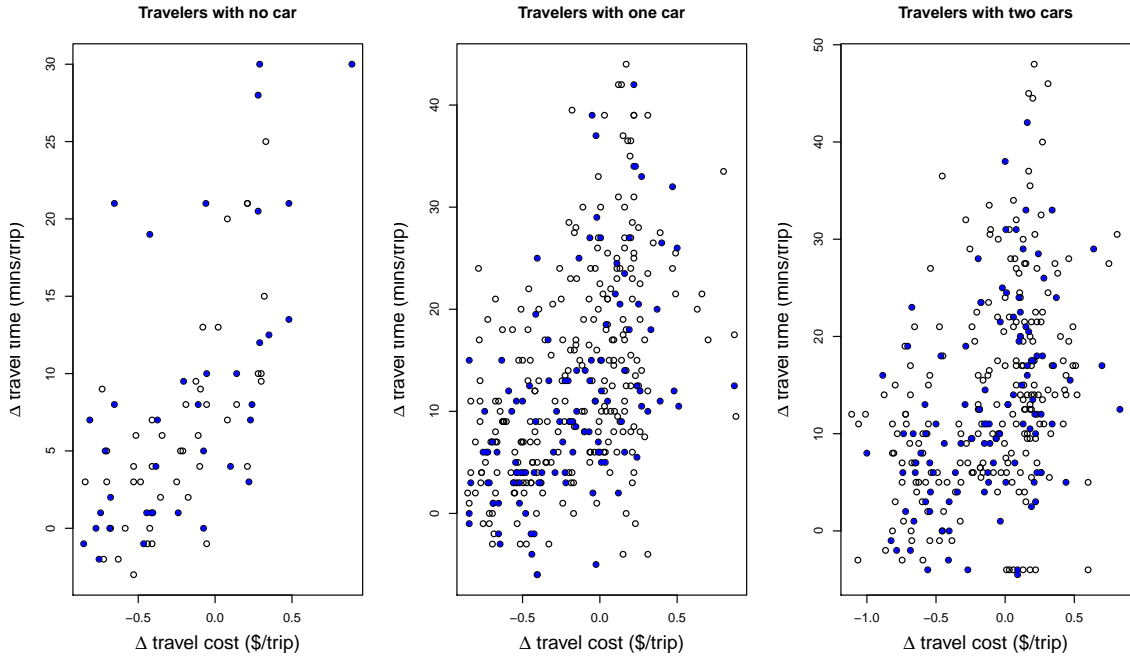
FIGURE 10. Scatter plot of DOVTT and DCOST for commuters with different number of cars at home: the open circles correspond to subjects that commute by auto while the solid (blue) points represent those who use public transit.

We briefly report results for the subsamples, $k \in \{0, 1, 2\}$, separately, focusing initially on the shape and dispersion of the estimated F_η distributions. For each subsample we contrast the discrete distribution delivered by the NPMLE with the contours of the smooth density produced by the Gautier and Kitamura estimator.

6.1. **Commuters without an Automobile.** There are 79 observations for commuters without a car. Despite having no car 16 still manage to commute to work by automobile. The lines determined by these realizations of (x_i, v_i) lead to a partition of $\mathbb{R}^2$ into 2992 polygons, of these only 112 are locally maximal and therefore act as potential candidates for positive mass assigned by the NPMLE of F_η. In Figure 11 we compare the estimates of F_η produced by the NPMLE and the deconvolution estimator of Gautier and Kitamura. The solid (red) points in the figure represent the locations of the mass points identified by the NPMLE; the mass associated with each of these points is reported in Table 6. Only 11 of the 112 candidate polygons achieve mass greater that 0.001, determined by the NPMLE.

In contrast, the Gautier-Kitamura density contours are entirely concentrated near the origin. We have experimented quite extensively with the choice of tuning parameters for the Gautier-Kitamura estimator, eventually adopting a likelihood criterion for the choice of the sieve dimensions, T and TX, that are required. This criterion selects rather parsimonious models in this application, choosing $T = 2$ and $TX = 3$ for this subsample. See Table 5 of the

Appendix for further details on this selection. Selection of lower dimensional Fourier-Laplace expansions obviously yield more restrictive parametric specifications, however this greater degree of regularization seems to be justified by the commensurate reduction in variability of the estimator. Although the comparison is inherently somewhat unfair we note that the NPMLE achieves a log-likelihood of -28.16, while the Gautier-Kitamura estimate achieves -37.58.

The two points on the far left of Figure 11 constitute about 0.05 mass each and represent individuals who seem to be committed transit takers. A coefficient of, say $\eta_1 = -8$ would mean that the transit fare per trip would have to be 8 dollars per trip higher than the corresponding car fare to induce them to travel by car. The fact that the η_2 coordinates associated with these extreme points is about one, means that, since the z variable measures the transit time differential in its original scale of minutes, for such individuals a 10 minute time differential would be sufficient to induce them to commute by automobile.
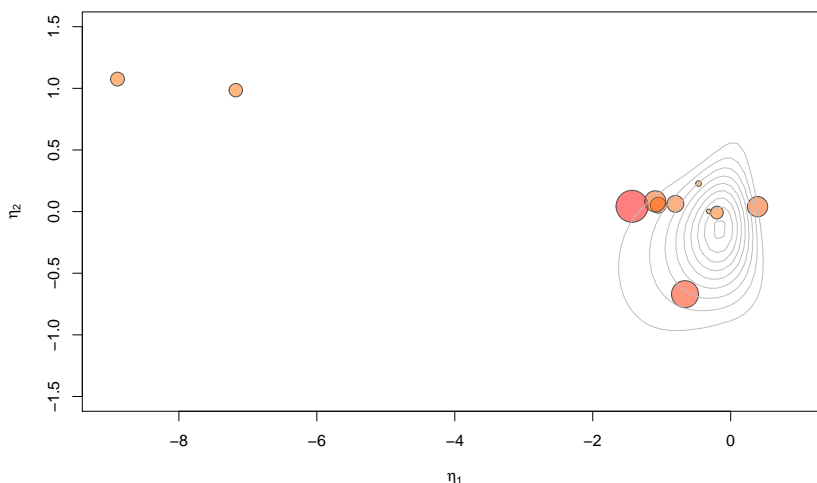

FIGURE 11. Two Estimates of the Random Coefficient Distribution F_η Based on the Subsample of Commuters with No Automobile: Shaded circles represent the interior points of polygons with positive mass as estimated by the NPMLE. The area inside the circles is proportional to estimated mass. Table 6 in the Appendix reports the NPMLE results in greater detail. Grey contour lines depict the density contours of the Gautier-Kitamura estimator using Fourier-Laplace tuning parameters $T = 2$ and $TX = 3$ selected by the log-likelihood criterion.

6.2. **Commuters with One Automobile.** There are 355 commuters who have one automobile of which 302 commute by car. The hyperplane arrangement determined by this subsample of pairs (x_i, v_i) yields a tessellation of $\mathbb{R}^2$ into 55549 distinct polygons of which there are 1272 with locally maximal counts. Figure 12 displays the estimated mass points of

the NPMLE and the contour plot the Gautier-Kitamura density estimate as in the preceed-
ing figure. As for the subsample without an automobile, the NPMLE mass is considerably
more dispersed than the Gautier-Kitamua contours. This may be partly attributed to the
rather restrictive choice of the tuning parameters, $T = 3$ and $TX = 3$, dictated by the like-
lihood criterion. Again, a more detailed tabulation of how the NPMLE mass is allocated
is available in Table 6. It may suffice here to note that while most of the NPMLE mass is
again centered near the origin, there is about 0.10 mass at $(\eta_1, \eta_2) \approx (9.7, -0.24)$ and an-
other, roughly, 0.05 probability with $\eta_1 < -12$. The Gautier-Kitamura contours are again
much more concentrated around the origin. These differences are reflected in substantial
differences in predicted outcomes and estimated marginal effects.
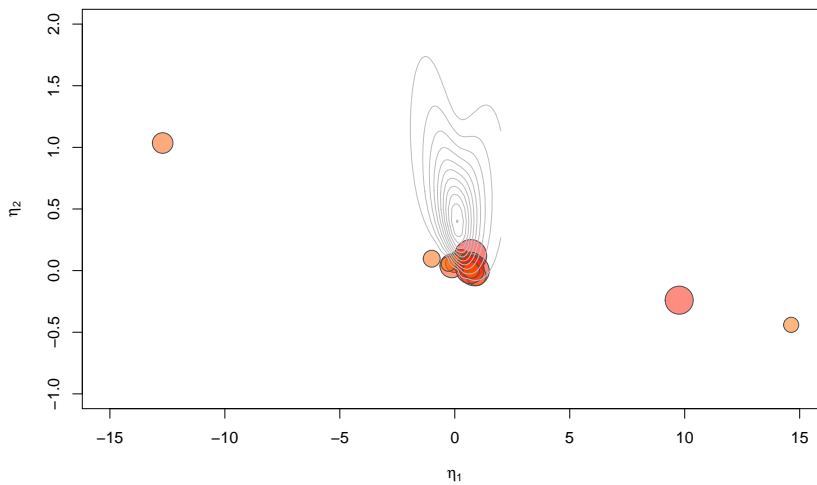

FIGURE 12. Two Estimates of the Random Coefficient Distribution F_η
Based on the Subsample of Commuters with One Automobile: Shaded circles
represent the interior points of polygons with positive mass as estimated by
the NPMLE. The area inside the circles is proportional to estimated mass.
Table 6 in the Appendix reports the NPMLE results in greater detail. Grey
contour lines depict the density contours of the Gautier-Kitamura estimator
using Fourier-Laplace tuning parameters $T = 2$ and $TX = 3$ selected by the
log-likelihood criterion.

6.3. **Commuters with Two Automobiles.** There are 316 travellers with 2 cars of which
303 commute to work by automobile. Of the 44662 polygons for this subsample there are
only 288 with locally maximal counts. Figure 13 depicts the mass points of the NPMLE
and the contours of the Gautier-Kitamura estimate for this subsample. The disperson of
the threshhold parameter η_1 is considerably smaller than for the zero and one car subsam-
ples, but it is still the case that the NPMLE is more dispersed that the Gautier-Kitamura
estimate in this dimension. Curiously, the Gautier-Kitamura estimate places most of its
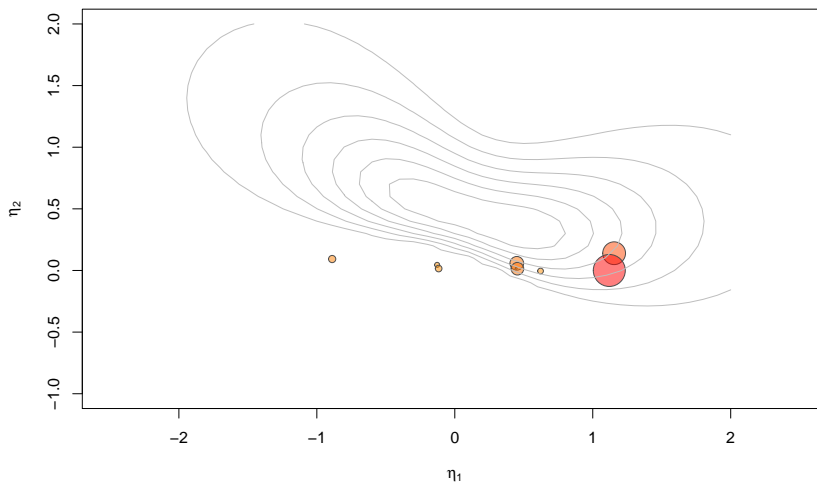
FIGURE 13. Two Estimates of the Random Coefficient Distribution F_η Based on the Subsample of Commuters with Two Automobiles: Shaded circles represent the interior points of polygons with positive mass as estimated by the NPMLE. The area inside the circles is proportional to estimated mass. Table 6 in the Appendix reports the NPMLE results in greater detail. Grey contour lines depict the density contours of the Gautier-Kitamura estimator using Fourier-Laplace tuning parameters $T = 2$ and $TX = 3$ selected by the log-likelihood criterion.

mass well above any of the NPMLE mass points. This may again be a consequence of the low dimensionality of the Fourier-Laplace expansion, which is selected as $T = 2$ and $TX = 3$ by the likelihood criterion.

6.4. **Marginal Effects.** We consider two scenarios for evaluating marginal effects based on estimates of the quantities,

$$\Delta_z(z_0, v_0, \Delta z) = \mathbb{P}(y = 1 \mid v = v_0, z = z_0) - \mathbb{P}(y = 1 \mid v = v_0, z = z_0 - \Delta z)$$
$$\Delta_v(z_0, v_0, \Delta v) = \mathbb{P}(y = 1 \mid v = v_0, z = z_0) - \mathbb{P}(y = 1 \mid v = v_0 - \Delta v, z = z_0).$$

The value $\Delta_z(z_0, v_0, \Delta z)$ measures the marginal effect of reducing out-of-vehicle travel time by Δz minutes/trip; the value $\Delta_v(z_0, v_0, \Delta v)$ measures the marginal effect of reducing the transit fare by Δv dollars holding transportation time constant. In each case, we fix the initial values (z_0, v_0) at the 75-th quantiles for the subsample of individuals who drive to work. Figures 14 and 15 depict the marginal effect of fare reduction and commute time reduction, respectively, conditional on automobile ownership.

As discussed in Section 4, for any fixed n, the NPMLE $\hat{F}_n$ assigns probability mass $\{\hat{p}_j\}_{j=1:M}$ to polytopes $\{C_j\}_{j=1:M}$ that define the partition of the parameter space determined by the hyperplane arrangement, not to specific points. This feature of the
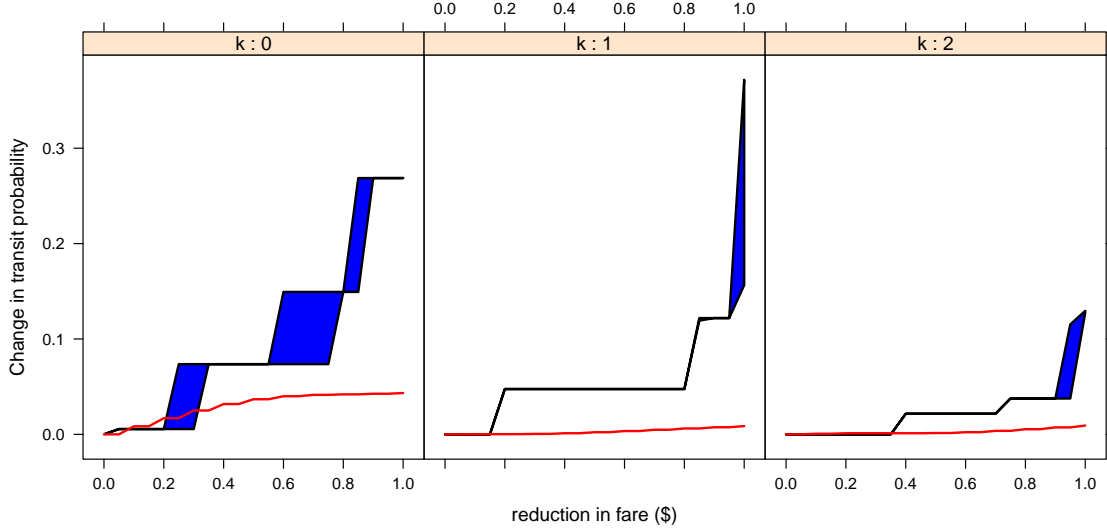
FIGURE 14. Set Valued Estimates of Marginal Effect for Transit Fare Reduction: The shaded solid regions represent the NPMLE set-valued estimates of the marginal effect of reducing the transit fare on the probability of choosing the transit option, the (red) line represents the corresponding estimates from the Gautier-Kitamura fit.

NPMLE naturally leads to a set valued estimator for marginal effects. Suppose we would like estimate $\Delta_z(z_0, v_0, \Delta z)$. Denoting the halfspace determined by any point $(1, z, v)$ by $H^+(v, z) := 1\{(\eta_1, \eta_2) : \eta_1 + \eta_2 z - v \geqslant 0\}$, it is easy to see that the set estimator for $\mathbb{P}(y = 1 \mid v = v_0, z = z_0)$ can be expressed as,

$$\mathbb{P}_{\hat{F}_n}(H^+(v_0, z_0)) \in [\hat{L}_n(v_0, z_0), \hat{U}_n(v_0, z_0)]$$

with

$$\hat{L}_n = \sum_{j=1}^{M} 1\{C_j \subseteq H^+(v_0, z_0))\hat{p}_j$$

and

$$\hat{U}_n = \sum_{j=1}^{M} 1\{C_j \subseteq H^+(v_0, z_0))\hat{p}_j + \sum_{j=1}^{M} 1\{C_j \nsubseteq H^+(v_0, z_0), C_j \cap H^+(v_0, z_0) \neq \emptyset\}\hat{p}_j$$

The set valued estimator for the marginal effect is therefore,

$$\hat{\Delta}_z(z_0, v_0, \Delta z) \in [\hat{L}_n(z_0, v_0) - \hat{U}_n(z_0 - \Delta z, v_0), \hat{U}_n(z_0, v_0) - \hat{L}_n(z_0 - \Delta z, v_0)]$$

Figures 14 and 15 report these bounds for different values of Δz and Δv.

The corresponding marginal effects for the Gautier-Kitamura estimates are depicted as the dotted red curves in this figure. The concentration of the Gautier-Kitamura $\hat{F}_\eta$ near the origin implies marginal effects that are considerably smaller than those implied by the
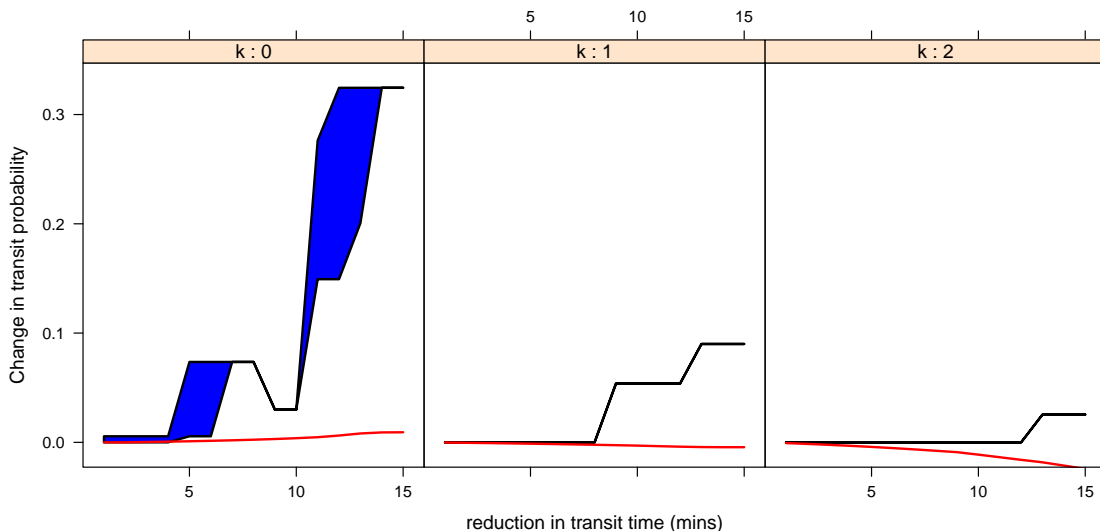
FIGURE 15. Set Valued Estimates of Marginal Effect for Transit Time Reduction: The shaded solid regions represent the NPMLE set-valued estimates of the marginal effect of reducing the transit time in minutes on the probability of choosing the transit option, the (red) line represents the corresponding estimates from the Gautier-Kitamura fit.

NPMLE results. For both the fare and transit time effects the Gautier-Kitamura estimates. Car ownership is clearly an important influence especially on the marginal effects of time savings for commuters without a car; while there is essentially no marginal effect for commuters with two cars.

6.5. **Single Index Model.** As a final comparison, we reconsider the single index model described in Section 2 where the parameter η_2 is treated as fixed and there is only a random intercept effect,

$$\mathbb{P}(y_i = 1 \mid x_i, v_i, \mathsf{AUTOS}_i = k) = \int 1\{\eta_{1i} + z_i\eta_2 - v_i \geqslant 0\}dF_{\eta_{1,k}}.$$

We consider several semiparametric estimators that make no distributional assumption on $F_{\eta_{1,k}}$ as well as the parametric probit estimator that presumes that $F_{\eta_{1,k}}$ is standard Gaussian. Since we can only identify $F_{\eta_{1,k}}$ up to scale, we again normalize the coefficient for v_i to be 1. We consider the kernel-smoothing based estimator proposed by Klein and Spady (1993) and the score estimator proposed in Groeneboom and Hendrickx (2018) based on the nonparametric maximum likelihood estimator of $F_{\eta_{1,k}}$ as in Cosslett (1983). The former estimator requires a choice of a bandwidth for the kernel estimate, whereas the latter is free of tuning parameters. The Klein-Spady estimates are based on the implementation in the R package np of Hayfield and Racine (2008) using a Gaussian kernel. The bandwidth is chosen automatically via a likelihood-based cross-validation criterion. The estimation results are reported in Table 4 together with the probit model estimates. In comparison,

we also include in the last column the log-likelihood of the random coefficient model where η_2 is allowed to be heterogeneous across individuals.

A virtue of the single index representation is that it is possible to estimate standard errors for the fixed parameter estimate $\hat{\eta}_2$, which appear in the table in parentheses under their coefficients. However, as is clear from the foregoing figures and the log likelihood values of Table 4 these standard errors require a willing suspension of disbelief in view of the apparent heterogeneity of the NPMLE estimates of the bivariate model.

Cars	Groeneboom-Hendrickx		Klein-Spady		Probit		NPMLE(η_1, η_2)
	$\hat{\eta}_2$	logL	$\hat{\eta}_2$	logL	$\hat{\eta}_2$	logL	logL
0	0.026 (0.022)	-32.87	-0.396 (0.026)	-37.60	0.034 (0.021)	-37.420	-29.55
1	0.018 (0.006)	-121.71	0.034 (0.007)	-131.71	0.028 (0.010)	-130.84	-112.32
2	0.030 (0.009)	-47.33	0.003 (0.003)	-51.85	0.048 (0.019)	-51.80	-46.13

TABLE 4. Estimates for η_2 of the single index model for households having different numbers of vehicles. The semiparametric and parametric probit estimates normalize the coefficient of ν to be 1. The last column reports the log-likelihood of the NPMLE for the bivariate model in which η_2 is allowed to be individual specific. The Klein-Spady estimator is implemented with the `npindexbw` and `npindex` functions of the `np` package. We use a Gaussian kernel and the bandwidth is chosen based on optimizing the likelihood criteria for both parameters and the bandwidth through leave-one-out cross validation. The BFGS method was used for optimization with 20 randomly chosen starting initial values. The Groeneboom-Hendrickx results were computed with the `GH` function from the R package `RCBR`.

7. Conclusion

Random coefficient binary response models estimated by the nonparametric maximum likelihood methods of Kiefer and Wolfowitz (1956) as originally proposed by Cosslett (1983) and extended by Ichimura and Thompson (1998) offer a flexible alternative to established parametric binary response methods. Modern convex optimization methods combined with recent advances in the algebraic geometry of hyperplane arrangements provide efficient computational techniques for the implementation of these methods. Further investigation of these methods is clearly warranted.

References

ALEXANDERSON, G., AND J. WETZEL (1981): "Arrangements of Planes in Spaces," *Discrete Mathematics*, 34, 219–240.

ANDERSEN, E. D. (2010): "The Mosek Optimization Tools Manual, Version 6.0," Available from `http://www.mosek.com`.

AVIS, D., AND K. FUKUDA (1996): "Reverse search for enumeration," *Discrete Applied Mathematics*, 65, 21–46.

BUCK, R. (1943): "Partition of Space," *The American Mathematical Monthly*, 50, 541–544.

CHEN, J. (2017): "Consistency of the MLE under mixture models," *Statistical Science*, 32, 47–63.

CHESHER, A., AND A. ROSEN (2014): "An instrumental variable random-coefficient model for binary outcomes," *Econometrics Journal*, 17, 1–19.

COSSLETT, S. (1983): "Distribution-free maximum likelihood estimator of the binary choice model," *Econometrica*, 51, 765–782.

EDELSBRUNNER, H., R. SEIDEL, AND M. SHARIR (1993): "On the zone theorem for hyperplane arrangements," *SIAM Journal of Computing*, 22, 418–429.

FRIBERG, H. A. (2012): "Users Guide to the R-to-Mosek Interface," Available from `http://rmosek.r-forge.r-project.org`.

GAUTIER, E., AND Y. KITAMURA (2013): "Nonparametric estimation in random coefficients binary choice models," *Econometrica*, 81, 581–607.

GROENEBOOM, P., AND K. HENDRICKX (2018): "Current Status Linear Regression," *Annals of Statistics*, 46, 1415 – 1444.

GROENEBOOM, P., AND G. JONGBLOED (2014): *Nonparametric Estimation under Shape Constraints: Estimators, Algorithms and Asymptotics*. Cambridge University Press.

GROENEBOOM, P., G. JONGBLOED, AND B. WITTE (2010): "Maximum smoothed likelihood estimation and smoothed maximum likelihood estimation in the current status model," *Annals of Statistics*, 38, 352–387.

GU, J., AND R. KOENKER (2016): "On a Problem of Robbins," *International Statistical Review*, 84, 224–244.

——— (2018): *RCBR: An R Package for Binary Response with Random Coefficients*. Coming soon to your favorite CRAN mirror.

HAYFIELD, T., AND J. RACINE (2008): "Nonparametric Econometrics: The np package," *Journal of Statistical Software*, 27, 1–32.

HOROWITZ, J. (1993): "Semiparametric estimation of a work-trip mode of choice model," *Journal of Econometrics*, 58, 49–70.

ICHIMURA, H., AND T. THOMPSON (1998): "Maximum likelihood estimation of a binary choice model with random coefficients of unknown distribution," *Journal of Econometrics*, 86, 269–295.

KIEFER, J., AND J. WOLFOWITZ (1956): "Consistency of the Maximum Likelihood Estimator in the Presence of Infinitely Many Incidental Parameters," *The Annals of Mathematical Statistics*, 27, 887–906.

KLEIN, R., AND R. SPADY (1993): "An Efficient Semiparametric Estimator for Binary Response Models," *Econometrica*, 61, 387–421.

KOENKER, R., AND J. GU (2017): "REBayes: An R Package for Empirical Bayes Mixture Methods," *Journal of Statistical Software*, 82, 1–26.

KOENKER, R., AND I. MIZERA (2014): "Convex Optimization, Shape Constraints, Compound Decisions and Empirical Bayes Rules," *J. of Am. Stat. Assoc.*, 109, 674–685.

LINDSAY, B. (1983): "The Geometry of Mixture Likelihoods: A General Theory," *Annals of Statistics*, 11, 86–94.

MAATHUIS, M. H. (2005): "Reduction Algorithm for the NPMLE for the distribution function of bivariate interval censored data," *J. of Computational and Graphical Statistics*, 14, 352–362.

MANSKI, C. (1975): "Maximum Score Estimation of the Stochastic Utility Model," *Journal of Econometrics*, 3, 205–228.

R CORE TEAM (2018): *R: A Language and Environment for Statistical Computing*.

RADA, M., AND M. ČERNÝ (2018): "A new algorithm for enumeration of cells of hyperplane arrangements and a comparison with Avis and Fukuda's reverse search," *SIAM Journal of Discrete Mathematics*, 32, 455–473.

SLEUMER, N. (1998): "Output-Sensitive cell enumeration in hyperplane arrangements," in *Algorithm Theory - SWAT'98*, ed. by S. Arnborg, and L. Ivansson, pp. 300–309. Springer-Verlag Berlin Heidelberg.

ZASLAVSKY, T. (1975): *Facing up to arrangements: Formulas for partitioning space by hyperplanes*, vol. 154 of *Memoirs of the AMS*. American Mathematical Society.

Appendix A. Computational Details

All of the figures and tables presented here can be reproduced in the R language, R Core Team (2018), with code provided by the second author. Full algorithmic details and documentation are available in the R package `RCBR`, of Gu and Koenker (2018), which in turn relies upon the R packages `REBayes` and `Rmosek` of Koenker and Gu (2017) and Friberg (2012).

Appendix B. Supplementary Tables

Two supplementary tables are provided in this section. Table 5 reports log likelihood values for various choices of the tuning parameters of the Gautier-Kitamura estimator for the modal choice application. The contour plots for the Gautier-Kitamura estimates appearing in the main text are based on tuning parameters maximizing log likelihood as reported in this table. Table 6 reports the location and mass of the NPMLE estimates for each subsample of the modal choice data; only points with mass greater than 0.001 are reported. Note, once again, that locations are arbitrary interior points within the polygons optimizing the log likelihood.

T	TX = 3	TX = 5	TX = 10	TX = 15	TX = 20
0 Cars					
1	−39.33	−41.27	−40.94	−41.54	−41.13
2	−39.16	−40.28	−41.23	−40.18	−39.13
3	−39.54	−40.64	−40.75	−39.51	−39.07
4	−40.45	−41.12	−40.47	−40.13	−40.25
5	−41.29	−41.83	−41.02	−41.19	−41.58
7	−41.96	−43.46	−43.73	−42.81	−42.56
9	−42.81	−45.48	−47.13	−45.96	−45.25
1 Cars					
1	−223.33	−158.55	−178.90	−195.51	−163.35
2	−179.44	−153.06	−157.35	−165.20	−153.68
3	−145.51	−146.91	−162.93	−165.86	−166.01
4	−148.49	−151.01	−162.31	−162.19	−180.44
5	−151.37	−154.96	−169.23	−168.51	−198.44
7	−161.38	−170.41	−191.81	−206.85	−229.93
9	−168.29	−179.99	−198.82	−211.48	−230.02
2 Cars					
1	−91.20	−164.31	−167.78	−126.56	−93.70
2	−89.88	−126.42	−172.32	−143.76	−115.74
3	−110.17	−141.13	−185.35	−165.72	−142.57
4	−128.33	−152.74	−188.94	−162.99	−143.09
5	−135.02	−154.10	−177.19	−148.85	−132.89
7	−135.22	−146.45	−155.38	−132.70	−123.55
9	−137.42	−145.49	−155.21	−139.99	−128.56

TABLE 5. Log-likelihood of the Gautier-Kitamura estimator for various values of the Fourier-Laplace series truncation parameters

No Car			One Car			Two Cars		
η_1	η_2	p	η_1	η_2	p	η_1	η_2	p
−1.4300	0.0429	0.2743	0.6917	0.1217	0.1300	1.1200	0.0000	0.5000
−0.6625	−0.6700	0.1955	0.8446	−0.0008	0.1153	1.1550	0.1400	0.2533
−1.0942	0.0830	0.1194	9.7600	−0.2400	0.0999	0.4495	0.0580	0.0918
0.3900	0.0400	0.1099	0.6666	0.0081	0.0999	0.4540	0.0143	0.0777
−0.8019	0.0628	0.0757	0.6790	0.0430	0.0875	−0.8889	0.0928	0.0254
−1.0500	0.0520	0.0680	−0.1271	0.0385	0.0717	−0.1170	0.0157	0.0216
−8.8900	1.0750	0.0512	0.2500	0.0800	0.0624	0.6216	−0.0045	0.0160
−7.1750	0.9850	0.0482	−12.7050	1.0350	0.0538	−0.1280	0.0455	0.0123
−0.1994	−0.0078	0.0437	0.9422	−0.0441	0.0475	0.4450	0.0175	0.0019
−0.4663	0.2275	0.0086	−0.0081	0.0588	0.0415			
−0.3177	0.0018	0.0055	0.5825	0.0650	0.0407			
			−1.0050	0.0967	0.0362			
			0.7086	0.0042	0.0346			
			14.6300	−0.4400	0.0291			
			−0.2789	0.0536	0.0271			
			0.1650	0.0942	0.0196			
			0.8411	−0.0077	0.0027			

TABLE 6. Mass points of the estimated distribution of coefficients for commuters: The first two columns in each panel indicate interior points of cells containing the estimated mass given by the third column of each panel. Only mass points with mass greater than 0.001 are displayed.